OCA-B/Pou2af1 Expression in Mouse T Cells Promotes PD-1 Blockade-Induced Autoimmunity but is Dispensable for Anti-Tumor Immunity

Junhong Du[1,2], Asit K. Manna[1,2], Erik P. Hughes[1,2], Paulla Bisoma[1,2], Kimberley J. Evason[1,2], Arabella Young[1,2], W. David Wilson[3], Abdelbasset A. Farahat[4,5], Dean Tantin[1,2]

[1]Department of Pathology, University of Utah School of Medicine, Salt Lake City, UT, 84112, USA.

[2]Huntsman Cancer Institute, University of Utah School of Medicine, Salt Lake City, UT, 84112, USA.

[3]Department of Chemistry, Georgia State University, Atlanta, GA 30303, USA.

[4]Master of Pharmaceutical Science Program, California North State University, Elk Grove CA 95757, USA.

[5]Department of Pharmaceutical Organic Chemistry, Faculty of Pharmacy, Mansoura University, Mansoura 35516, Egypt

Correspondence to Dean Tantin: dean.tantin@path.utah.edu

Short title: OCA-B Promotes PD-1 Blockade-Triggered Diabetes

Keywords OCA-B/Pou2af1; Type-1 diabetes; Non-obese diabetic mouse; tumor immunity; MC38

Conflicts of interest statement: The authors have declared that no conflict of interest exists

Words in abstract: 225

Words main text: 11,201

Total main display items: 6

Abstract

The transcription coregulator OCA-B promotes $CD4^+$ T cell memory recall responses and autoimmunity. OCA-B T cell deletion blocks spontaneous T1D onset in non-obese diabetic (NOD) mice and blunts T1D in a subset of more aggressive models. However, the role of OCA-B in diabetes induced by treatment with checkpoint blockade therapies, and the role of OCA-B in the control of tumors with and without α-PD-1 treatment, has not been studied. We show that deletion of OCA-B in T cells fully insulates 8-week-old non-obese diabetic (NOD) mice against α-PD-1 antibody-induced diabetes induction and partially protects 12-week-old mice. Salivary/lacrimal gland infiltration and inflammation were also reduced. Protection was associated with a block in the differentiation of progenitor exhausted $CD8^+$ T cells (T_{PEX}) into terminally exhausted $CD8^+$ T cells (T_{EX}). We show that OCA-B T cell loss preserves anti-tumor immune responses following PD-1 blockade therapy in a variety of tumor cell lines. These findings point to a potential therapeutic window in which pharmaceuticals that target OCA-B could be used to block the emergence of both spontaneous and checkpoint blockade-induced autoimmunity while minimally affecting anti-tumor immune responses. We develop first-in-class small molecule inhibitors of Oct1/OCA-B transcription complexes and show that administration into NOD mice also blocks diabetes emergence following α-PD-1 treatment. These results identify OCA-B as a promising therapeutic target for the prevention of autoimmunity and immune-related adverse events (irAEs).

Introduction

Type 1 diabetes (T1D) affects 1.8 million people in the United States and is increasing worldwide [1-3]. It is characterized by autoimmune destruction of pancreatic β cells and consequent inability to produce insulin [4]. While T1D symptoms can be managed with insulin injections, they must be taken for life. Transplantation of islets of Langerhans can restore insulin-independence to T1D patients, but results in reactivation of islet-specific memory cells T cells, β cell destruction and transplant rejection [5,6]. Similarly, engraftment of islets from non-obese diabetic (NOD) mice with severe combined immunodeficiency (NOD.SCID) into diabetic NODs briefly restores normoglycemia, but results in robust memory autoimmune responses and complete loss of grafted islet function in 10-14 days [7]. Human therapies aim to minimize graft rejection or block the initial emergence of T1D in at-risk patients altogether while sparing normal immune function [8].

In humans, α-PD-1 therapy as well as therapies directed against a number of other inhibitory T cell receptors (immune checkpoint inhibitors or ICIs) are now used for treatment of a variety of cancer indications [9-11]. The development and wide adoption of ICIs has resulted in a concomitant increase in associated unwanted immune-related adverse events, or irAEs, affecting a variety of tissues (e.g., skin, rheumatoid, pulmonary, gut, cardiac), some of which can be permanent [9,12-19]. IrAEs include endocrinopathies such as thyroiditis [20], and less frequently hypophysitis, autoimmune diabetes and other diseases [15,17]. A critical gap in the field is the identification of treatment strategies that block the emergence of irAEs while preserving anti-tumor immunity.

Polymorphisms in the *HLA-DR* and *HLA-DQ* genes encoding MHC class II have the strongest genetic influence on T1D, accounting for 40-50% of familial risk [21]. These findings implicate $CD4^+$ T cells as primary drivers of pathogenesis. $CD4^+$ T cells direct other cell types such as $CD8^+$ T cells and macrophages to infiltrate pancreatic islets and cause β-cell destruction [22]. Consistent with these findings, transient T cell depletion using α-CD3ε antibodies (Teplizumab-mzwv) significantly delays T1D onset in at-risk individuals in human clinical trials [23,24]. Though promising, such treatments are limited by the resulting global immunosuppression. An ideal alternative would selectively deplete pathogenic T cell function while preserving beneficial immune function, including immunity against tumors.

OCA-B is a B cell- and T cell-restricted transcription coactivator [25,26]. In $CD4^+$ T cells, OCA-B docks with the transcription factor Oct1 (gene symbol *Pou2f1*) to regulate targets including *Il2*, *Ifng*, *Icos*, *Csf2* (*Gmcsf*) and *Tbx21* (*Tbet*) [27,28]. Unlike transcription factors such as NFAT, AP-1 and NF-κB, OCA-B controls the expression of these genes specifically during repeated antigen exposures [27,28]. Agents targeting this pathway would selectively inhibit over-active T cell responses to antigen re-exposure but preserve acute immune response. Consistent with this prediction, in the absence of either OCA-B or its cognate transcription factor Oct1/Pou2f1, primary T cell responses to systemic and glial-tropic viruses (LCMV and JHMV, respectively) and viral clearance are normal [26,29], however fewer central memory (T_{CM}) $CD4^+$ T cells form, and those that do respond poorly to antigenic re-challenge [26,28]. Three studies directly link polymorphisms in the human *OCAB* (*POU2AF1*) locus with autoimmune disease [30-32]. Human polymorphisms affecting Oct1 (and therefore OCA-B) binding to the *TNFA* and *CTLA4* loci are associated with inflammatory bowel disease and systemic lupus erythematosus, respectively [33,34]. More recent work identified additional polymorphisms in Oct1 binding sites within the human *IL13*, *IL18* and *HLA-C* loci [35-37]. Additionally, two meta-analyses show a strong association between Oct1/OCA-B binding site polymorphisms and autoimmunity including T1D[38,39]. Collectively, these studies link OCA-B with human autoimmunity.

OCA-B loss in T cells protects mice against spontaneous T1D onset [40]. Single-cell RNA-sequencing (scRNA-seq) reveals that protection is associated with loss of autoreactive clones but maintenance of the overall pancreatic islet immune architecture [40]. These findings suggest that targeting OCA-B could be used to treat T1D early in the disease course while sparing baseline immunity. OCA-B's lymphoid-restricted expression pattern [25,26], its dispensability for primary antiviral responses [26,28,29], and its specificity for Oct1/Pou2f1 and Oct2/Pou2f2 complexes with DNA [41-43] make it a promising therapeutic target that could be used to specifically block autoreactive $CD4^+$ T cells while sparing normal immunity. OCA-B peptide mimics linked to membrane-penetrating peptides can reduce inflammation and hyperglycemia in recent-onset T1D NOD mice, but also show significant toxicity [40]. An outstanding question is whether OCA-B can be successfully targeted by more drug-like small molecules. It also remains to be determined if OCA-B promotes diabetes driven by ICI therapy, and/or if OCA-B promotes anti-tumor immunity, including that promoted by ICI.

Here, we show that OCA-B in T cells promotes the emergence of autoimmune diabetes following ICI administration in NOD mice, while being dispensable for anti-tumor immune responses or tumor regression following ICI administration. We develop small molecules that effectively disrupt Oct1:OCA-B complexes in vitro and disrupt OCA-B's transcription functions in cultured cells. We show that administration of these compounds to NOD mice blocks the emergence of diabetes and other endocrinopathies following ICI administration, with in vivo efficacy tracking with activity in vitro. Collectively, the findings indicate that OCA-B promotes diabetes development following ICI treatment, and that targeting OCA-B could be used to block irAEs following ICI while sparing anti-tumor immunity.

Results

OCA-B T cell knockout protects NOD mice against diabetes induced by α-PD-1 antibody treatment

T cell conditional OCA-B loss protects NOD mice against spontaneous T1D [40]. Modulating the PD-1 pathway induces diabetes and other endocrinopathies in NOD mice [44-47]. To test the effect of OCA-B T cell loss in diabetes induced by PD-1 blockade, we treated 8-week-old male NOD mice with four injections of α-PD-1 antibody. OCA-B loss in T cells completely blocked α-PD-1-induced diabetes development (Figure 1A-B). Treatment of 12-week-old female NOD mice with α-PD-1 antibodies resulted in less complete protection, with half the mice failing to develop diabetes and the other half showing delayed onset (Supp. Figure 1A-B). Flow cytometry revealed a significant reduction in $CD45^+$ leukocytes in α-PD-1 antibody treated knockout mice (Figure 1C-D). We also observed a skewing from $CD8^+$ to $CD4^+$ T cells in the islets of 8-week-old knockouts (Figure 1E-F), consistent with changes in immune profiles reflecting diabetes progression [22]. At 12 weeks, islet PD-1^+TIM-3^+ $CD8^+$ T cells were decreased in the OCA-B deficient condition (Supp. Figure 1C-D). PD-1 blockade is known to normally induce exhausted $CD8^+$ T cell proliferation and differentiation in the pancreas, promoting the expansion of both T_{PEX} and T_{EX} cells but also skewing the islet total population in favor of T_{EX} [22]. The finding of decreased TIM-3 expression could therefore be explained if OCA-B loss blocks this pathogenic maturation. To test this, we used SLAMF6 and CD39 to distinguish T_{PEX} and T_{EX} $CD8^+$ T cells at both 8 and 12 weeks. OCA-B loss resulted in a marked retardation in the ability of PD-1^+CD8^+ T_{PEX} cells within the islets of 8-week-old mice to differentiate into T_{EX} (Figure 1G-H). Similar findings were made at 12 weeks (Supp. Figure 1E-F). Cumulatively, these results indicate that OCA-B loss in T cells blocks the induction of diabetes by α-PD-1 treatment, and blocks the pathogenic maturation of a T_{PEX}-like T cell population in the pancreatic islets.

OCA-B T cell knockout maintains anti-tumor response and tumor control by ICI

To determine if OCA-B T cell loss has a corresponding effect on anti-tumor immunity, we used C57BL/6 and NOD mice OCA-B conditional knockout mice [26,40] with syngeneic tumor lines. In the C57BL/6 strain background we used two lines, B16F10 and MC38. Compared to littermate controls lacking the CD4-Cre driver, OCA-B loss had no effect on tumor growth of B16F10 tumors (Supp. Figure 2). This result was expected because B16 cells are “immune-cold” and do no elicit robust immune responses unless engineered to express specific antigens or unless multiple checkpoint-inhibiting antibodies are combined [48]. In contrast, “immune-hot” MC38 colon carcinoma cells exhibit significant control by T cells that can be augmented by α-PD-1 treatment [49]. MC38 tumor control was also preserved with OCA-B T cell loss either in the absence or presence of α-PD-1 antibody treatment (Figure 2A-B). Flow cytometry of cells from the tumor microenvironment (TME) showed equivalent $CD45.2^+$ leukocyte infiltration and ratios of $CD8^+$ to $CD4^+$ T cells with α-PD-1 treatment (Figure 2C-D). Similar percentages of $CD4^+$ and $CD8^+$ SLAMF6^+CD39^- and SLAMF6^-CD39^+ cells were also observed in the TME regardless of the status of OCA-B following α-PD-1 antibody treatment (Figure 2E-F). TIM-3 expression in tumor-infiltrating $CD4^+$ and $CD8^+$ was also equivalent (Figure 2G-H). Despite the lack of difference in T cell infiltration, exhaustion and tumor control, within the tumors there were interesting differences in both the $CD4^+$ and $CD8^+$ T_{CM}-like (CD62L^{hi}CD44^{hi}) and naïve-like (CD62L^{hi}CD44^{lo}) compartments (Supp. Figure 3). The significance of these differences for tumor control is currently unclear.

154 Because the protection from PD-1-induced diabetes was observed using NOD background mice, we
155 also assessed tumor responses using a syngeneic "immune-hot" 9495 sarcoma cell line [50], allowing
156 us to simultaneously measure diabetes incidence and tumor control in the same animals. α-PD-1
157 antibody treatment is effective in controlling 9495 tumor growth in syngeneic NOD mice [50]. To
158 minimize complications from induced diabetes and hyperglycemia, mice were administered insulin
159 pellets when glucose levels reached ≥250 mg/dL for two consecutive days to minimize complications
160 from induced diabetes and hyperglycemia. In these tumors, α-PD-1 antibody treatment was effective,
161 as expected [50]. Again, tumor control either with or without α-PD-1 treatment was equivalent regardless
162 of OCA-B status (Figure 3A-B). Simultaneously, in another cohort of mice with the same experiment
163 procedures performed, the OCA-B deficient group were again fully protected against diabetes (Supp.
164 Figure 4A). Similar to published work [50], control mice with induced diabetes exhibited superior tumor
165 control compared to uninvolved mice (Supp. Figure 4B-C). As with MC38 tumors in C57BL/6 mice,
166 $CD45^+$ leukocyte tumor infiltration, $CD8^+$ to $CD4^+$ T cell ratio, $CD8^+$ T cell activation, (Figure 3B-E) and
167 T_{PEX} to T_{EX} differentiation (Figure 3F-I) were equivalent. These findings indicate minimal differences in
168 anti-tumor immune responses to multiple syngeneic tumor lines in using mice with OCA-B T cell
169 knockout, indicating a divergence between anti-tumor immunity and the precipitation of irAEs that
170 could be leveraged therapeutically.

171 *Development of small molecule inhibitors of Oct1:OCA-B complexes*

172 The Oct1:OCA-B:DNA co-crystal structure [43] suggests multiple possible targeting strategies, including
173 rationally designed OCA-B peptide mimics (Figure 4A, upper lightning bolt) which are functional but
174 associated with toxicity in cells and mice due to the membrane penetrating peptide [40]. To identify novel
175 small molecule inhibitors, we used another strategy in which DNA minor groove-binding compounds
176 with specificity for the consensus octamer motif (5'ATGCAAAT) would disrupt Oct1:OCA-B
177 complexes. These inhibitors would dock on the underside of the DNA in the structure shown in Figure
178 4A (bottom lightning bolt) and would interfere with the unstructured Oct1 linker domain that also spans
179 the minor groove. We synthesized and tested 9 candidate minor groove-binding compounds with
180 specificity for the octamer motif. To test efficacy, we developed two cell-based assay systems. The
181 first is a transcription-based platform in which we stably transfected the human T cell line SupT1 to
182 express secreted nanoluciferase (nLuc) under the control of five Oct1/OCA-B binding sites. SupT1 T
183 cells express OCA-B at higher levels than, e.g. Jurkat cells, and at levels comparable to primary
184 thymocytes (Figure 4B). We generated a stable-transfected SupT1 clone expressing nLuc under the
185 control of five wild-type octamer sequences ("5×Oct") and a second using mutant sites incapable of
186 binding Oct1 and OCA-B ("5×Mut", Figure 4C). The 5×Oct clone produced substantial levels of
187 luciferase activity relative to empty vector-transduced controls, while the 5×Mut clone expressed lower
188 but still measurable activity (Figure 4D). Timecourse experiments show that 12- to 18-hr incubations
189 have not yet saturated nLuc activity and capture a dynamic range allowing both activators and
190 inhibitors to be detected (Figure 4E). We therefore chose 18-20 hr for all further experiments.
191 AlamarBlue readings are also taken to measure cell viability, using 2.5 μM staurosporine a positive
192 control for maximum toxicity. The treatment kills >98% of SupT1 cells within 18 hr and
193 correspondingly inhibits luciferase expression (Supp. Figure 5). Of the 9 candidate compounds two –
194 DB1033 (IC_{50}~25 mM, Figure 4F) and DB2232 (IC_{50}~20 mM, Supp. Figure 6A) – inhibited luciferase
195 activity without significantly affecting luciferase expression from the mutant cell line and without
196 significant toxicity. Other compounds such as DB2658 showed significant toxicity in the same screen
197 (Supp. Figure 6B) or were less active (e.g., DB2385, Supp. Figure 6C-H). The DB1033 structure is

198 shown in Figure 4G. Molecular docking indicated that DB1033 preferentially interacts with DNA minor
199 groove in the AAAT portion of the consensus octamer sequence, overlapping with the location of the
200 unstructured Oct1 linker domain (Figure 4H-I).

201 The reduce the possibility of off-target hits, we tested DB1033 compound activity using an orthogonal
202 cell-based method. We developed a nano-bioluminescence resonance energy transfer (NanoBRET)
203 assay that measures OCA-B's interaction with its cognate transcription factor Oct1. In this assay,
204 293T cells are co-transfected with an OCA-B construct carrying a HaloTag and an Oct1 construct
205 carrying an nLuc tag (Figure 5A). DB1033 again showed dose-dependent inhibition (Figure 5B),
206 indicating that DB1033 disrupts the interaction between Oct1 and OCA-B. To test this prediction at a
207 mechanism level, we used electrophoretic mobility shift assays (EMSA) with recombinant Oct1 DNA
208 binding domain and recombinant full-length OCA-B to measure formation of Oct1:OCA-B:DNA
209 complexes (Figure 5C). We used Cy5-conjugated double-stranded DNA to visualize complexes with
210 cognate DNA in native polyacrylamide gels. Labeled DNA was in excess relative to protein such that
211 changes in the ability to form a complex can be readily observed. Because of "caging effects",
212 changes in off-rates are not efficiently captured within a running native gel. Instead, in this assay
213 effects of an inhibitor on complex formation are likely generated during the incubation prior to gel
214 loading. We assembled the protein, DNA and buffer components on ice for 25 minutes in stringent
215 conditions (150 mM KCl), and incubated the mixture for a further 5 min at room temperature
216 ±compound prior to loading. Oct1 readily formed a complex with DNA that was augmented and
217 slightly supershifted in the presence of OCA-B, indicating the formation of a ternary complex (Figure
218 5D, lane 3). Inclusion of DB1033 efficiently disrupted complex formation in a dose-dependent manner
219 (lanes 4-7).

220 A complimentary in vitro assay uses differential scanning fluorimetry (nanoDSF) to measure
221 Oct1:OCA-B:DNA complex thermal stability. NanoDSF measures the gradual exposure of UV-
222 absorbing tyrosine side chains as proteins unfold with increasing temperature. We developed a
223 single-polypeptide chimeric molecule containing the Oct1 DNA binding domain fused to the first 44
224 amino acids of OCA-B, encompassing the structured part of OCA-B that contacts Oct1 (Figure 5E).
225 The first 15 amino acids of OCA-B do not appear to be well-structured and presumably serve as a
226 linker between the two molecules. AlphaFold 3 [51] predicts that the chimeric molecule folds similarly to
227 natural Oct1 and OCA-B on DNA (Figure 5F). The protein was expressed in *E. coli* with N-terminal 6-
228 His, consecutive C-terminal Twinstrep and FLAG tags. Following purification, the protein was found to
229 be mostly pure as assessed by Coomassie staining SDS-PAGE (Supp. Figure 7A). Size exclusion
230 chromatography indicated that the purified protein was mostly monodisperse, and EMSA indicated
231 that it was able to interact with consensus octamer DNA (Supp. Figure 7B-C). The presence of target
232 DNA strongly increased the stability of the chimeric protein in nanoDSF, as expected (Figure 5G),
233 while adding DB1033 in the presence of DNA destabilized the complex (Figure 5H). These findings
234 identify DB1033 as the best compound tested, indicate that DB1033 acts to disrupt Oct1:OCA-B
235 complexes on DNA, and establishes a pipeline for assessing molecules that modulate Oct1 and/or
236 OCA-B's interactions with one another and with DNA, their overall stability, and their transcriptional
237 functionality.

238 *Small molecule Oct1:OCA-B inhibitors block* α*-PD-1-indcued diabetes and other endocrinopathies in*
239 *NOD mice*

240 We treated 8-week-old male NOD mice with five *i.p.* injections of 15 mg/kg DB1033 or DB2232
241 simultaneously with α-PD-1 antibody treatment. 8 week-old male NOD.*Ocab*$^{fl/fl}$;CD4-Cre mice were

242 used as a positive control for protection. As with genetic OCA-B T cell knockout, DB1033 treatment
243 completely protected mice against diabetes emergence (Figure 6A-B). These results indicate 1) that
244 DB1033 is effective in protecting mice against α-PD-1 antibody-induced diabetes, and that 2) acute
245 inhibition at the same time as α-PD-1 antibody delivery is sufficient to protect mice against diabetes
246 development. DB1033 toxicity was negligible or low-level, as there was a trending but statistically
247 nonsignificant loss of weight associated with treated animals at endpoint (Figure 6C). Protection was
248 not only confined to the pancreatic islets but was also noted with salivary and lacrimal gland tissue,
249 where leukocyte infiltration was strongly reduced (Figure 6D-E). Importantly, the structurally related
250 DB2232 compound, which was inferior in cell-based assays, was also functionally inferior at
251 preventing diabetes (Supp. Figure 7D-F). These findings provide evidence of a structure-activity
252 relationship linking compound activity to OCA-B complex inhibition. In summary, the findings show
253 that OCA-B promotes the development of autoimmunity in NOD mice administered ICI while being
254 dispensable for anti-tumor immunity on multiple strain backgrounds, and identify small molecule
255 inhibitors that can be administered acutely and phenocopy the genetic knockout.

Discussion

Here we show that OCA-B expression in T cells promotes induced irAEs following ICI treatment while minimally affecting anti-tumor responses. We also, for the first time, show that a small molecule Oct1:OCA-B inhibitor phenocopies the protection against irAEs observed using the OCA-B T cell knockouts. The latter findings indicate that acute OCA-B inhibition is sufficient to protect against irAEs and suggest the existence of a therapeutic window in which OCA-B pharmacological targeting can be used to block autoimmunity while sparing baseline immune function, including immunity to tumors.

OCA-B is one of three tissue-restricted transcription coregulators known as OCA proteins: OCA-B, OCA-T1 and OCA-T2 [52]. Like the other two proteins OCA-B docks with the sequence-specific DNA binding POU transcription factors to regulate transcription [41-43]. The OCA-Ts are master regulators of tuft cells, and a therapeutic vulnerability in small cell lung cancers originating from this cell type [52]. OCA-B has important B cell-intrinsic functions including in the formation of germinal centers [53,54]. In T cells, OCA-B docks with the POU factor Oct1 to regulate target genes encoding cytokines and other immunomodulatory proteins [28]. Because OCA-B expression is 50-100-fold higher in B compared to T cells[26], a calibrated dose of competitive inhibitor could selectively block T cell functions while sparing B cell-intrinsic OCA-B functions. For all three proteins, whole-body null mice are healthy, viable and fertile [52,55,56], suggesting that they a good candidate drug targets, however no small molecules targeting OCA proteins have been described.

Multiple lines of evidence show that pathogenic human and mouse progenitor-like T cells promote and sustain autoimmunity including T1D [57-60]. In mice, OCA-B promotes pathogenesis in experimental autoimmune encephalomyelitis (EAE), a model of multiple sclerosis, through maturation of stem-like cells into encephalitogenic effectors [29]. These properties are T cell intrinsic. In a relapsing-remitting NOD.EAE model, OCA-B T cell-deficiency specifically protects mice from relapse [29]. On the NOD strain background, both OCA-B whole body and T cell-specific knockout block the onset of spontaneous T1D [40]. Using more aggressive T1D mouse models including CD25-mediated T_{reg} depletion and the CD8-restricted, autoreactive NY8.3 transgenic line revealed partial protection, while using the CD4-restricted BDC2.5 and CD8-restricted RIP-mOVA-OT-1 models showed no differences [40]. The protection conferred by OCA-B loss is therefore strongest in more chronic polyclonal models. These findings also reveal that OCA-B T cell loss does not result in global immunosuppression, which would result in broader protection. In female NOD mice with newly arisen T1D, intravenous administration of membrane-penetrating OCA-B peptide mimics briefly reverses elevated blood glucose, as well as pancreatic islet T cell infiltration and pro-inflammatory cytokine production [40]. In contrast to the pancreas, pLN showed no change in T cell numbers or percentages, but did show reduced T cell cytokine responses following self-peptide stimulation [40]. However, greater than three peptide injections was toxic, with mice exhibiting ruffled skin, moribund appearance and weight loss [40]. The Tat membrane-penetrating peptide is associated with acute toxicity that can be mitigated by spacing the dose[61-63].

The ability to trigger endocrine irAEs using α-PD-1 treatment in NOD mice presented an opportunity to test the OCA-B T cell loss of function model in different ways. First, to test the effect of OCA-B loss in an aggressive but physiologically relevant model of autoimmune diabetes. Second, to use the diabetes and other endocrinopathies as models for ICI-triggered irAEs. Third, to determine the role of OCA-B in anti-tumor immunity. We found that OCA-B T cell loss protected NOD mice against ICI-triggered diabetes. The effect of OCA-B loss was partially dependent on the age at which ICI was administered, with 8-week-old mice showing more complete protection compared to 12-week-old

mice. This finding is consistent with a model in which OCA-B loss protects NOD mice at multiple levels, one of which spans the 8-week timepoint and is PD-1 independent, and one of which spans the 12-week timepoint and is partially PD-1 dependent. Profiling the immune cells in these mice flow cytometrically indicated significant reduction in T_{EX}, and a concomitant increase in cells with a progenitor-like (SLAMF6^{hi}CD39^{lo}) phenotype.

In sharp contrast to the autoimmune protection conferred by OCA-B loss, immune responses and tumor control were preserved either with or without α-PD-1 treatment. No differences were observed using immune-cold B16F10 melanoma cells, as well as immune-hot MC38 colon carcinoma cells and 9495 basal cell carcinoma cells. Similar to the preservation of tumor control, loss of OCA-B in T cells preserves normal primary response and viral control following infection with either the acute strain of lymphocytic choriomeningitis virus (LCMV) or the glial-tropic β-coronavirus JHMV [26,28,29]. The normal T cell primary immune response phenotypes observed with Oct1 and OCA-B genetic deletion suggest the existence of a therapeutic window in which an OCA-B pharmaceutical could be used not just to block autoimmunity, but could be co-administered with ICIs to block irAEs while sparing immunity to viruses and tumors. A likely side effect of therapies targeting this pathway would be an inability of newly-generated memory CD4^{+} T cells to mount robust recall responses [26,28]. Our findings indicate that OCA-B promotes a memory-like population of CD4^{+} T cells important for immune responses to tumor re-challenge and relapse (manuscript in prep). An OCA-B inhibitor may therefore need to be withdrawn prior to any potential tumor relapse.

Despite the prevailing but erroneous idea that transcription factors are “undruggable,” there are multiple historical[61,64-66], and recent[67-81] counterexamples, the latter enabled by technologies such as PROTAC[82,83]. We show that systemic administration a small molecule inhibitor, DB1033, into NOD mice blocks the emergence of diabetes following the administration of α-PD-1 antibodies. These molecules disrupt Oct1:OCA-B:DNA complexes in cell culture and in vitro. The finding that DB1033 administration concomitant with α-PD-1 antibody treatment is sufficient to block the induction of diabetes and other endocrinopathies suggests that OCA-B actions close to the time of injection, and therefore spatially proximate to the pLNs and pancreatic islets, rather than development of auto-reactive T cells in an OCA-B deficient environment from the double-positive thymocyte stage onwards, mediates autoimmune protection. Moreover, we show that a structurally related compound, DB2232, that is inferior in attenuating OCA-B-dependent transcription in cell culture and in disrupting Oct1:OCA-B complexes in vitro is also functionally inferior at protecting NOD mice against ICI-triggered diabetes, strongly suggesting that these compounds act through OCA-B disruption. These reagents provide a conceptual milestone as a first-in-class small molecule Oct1/OCA-B inhibitor that can reduce autoimmunity. More work is necessary to develop superior and more drug-like small molecule inhibitors.

335 **Materials and Methods**

336 *Laboratory mice.* All mice used in this study were non-obese diabetic (NOD) background, with the
337 exception of B16-F10 and MC38 tumor injections which used C57BL/6 mice. *Pou2af1* (*Ocab*)
338 conditional (floxed) mice on the C57BL/6 and NOD backgrounds were generated as described
339 previously [26,40]. All animal experiments were approved by the University of Utah Institutional Animal
340 Care and Use Committee (IACUC approval 00001553).

341 *α-PD-1-induced diabetes.* 250 µg α-PD-1 (clone RMP1-14, Cat# BE0146, Bio X Cell) or rat IgG2a
342 isotype control (Cat# BE0089, Bio X Cell) was interperitoneally (*i.p.*) administered into NOD.*Ocab*$^{fl/fl}$ or
343 *Ocab*$^{fl/fl}$;CD4-Cre on day 0, 4, 8, and 12 (or on day 0, 4, 8, 12, and 16 as indicated). Antibody was
344 diluted in PBS for injection of 200 µL per mouse.

345 *Histology.* Salivary glands and lacrimal glands were isolated and fixed in 10% formalin. After 24-72 hr,
346 tissues were transferred to 70% ethanol and embedded in paraffin, sectioned at 5~7 µm, and H&E
347 staining was performed. Slides were examined and imaged using an Olympus BX53 microscope with
348 UPlanFL objectives, Olympus DP73 camera, and Olympus cellSens imaging software.

349 *Secondary lymphoid organ and tumor harvest.* Spleens and lymph nodes were ground and filtered
350 through a 70 µm nylon cell strainer (VWR #76327-100). Red blood cells were removed by
351 Ammonium-Chloride-Potassium (ACK) lysis buffer (10 mM $KHCO_3$, 150 mM NH_4Cl, and 0.1 mM
352 Na_2EDTA). MC38 tumors were manually disrupted by grinding between the frosted end of slide glass
353 in a 6-well plate with 3 mL of PBS plus 4% FBS, and filtered through a 40 µm nylon cell strainer (VWR
354 #76327-098). 9495 tumors were mechanically disrupted in 6-well-plate and digest in RPMI media
355 containing 16mg/mL collagenase D (Sigma-Aldrich #11088858001) and 10mg/mL Dnase (Sigma-
356 Aldrich #10104159001) at 37°C in CO_2 incubator for 45 minutes and filtered through a 40 µm nylon
357 cell strainer, spined in 37.5% percoll gradient, and red blood cells (RBCs) were lysed to produce
358 single-cell suspensions.

359 *Pancreatic islet harvest.* Lymphocytes were isolated based on a protocol from Jing et al. [84]. Pancreata
360 were harvested and perfused with collagenase 4 (Worthington #LS004188) at 37°C, and islets were
361 picked using a 10 µL pipette. Islet single-cell suspensions were obtained by vortexing in cell
362 dissociation buffer (ThermoFisher Scientific #13151014).

363 *Flow cytometry.* Single-cell samples were stained with antibodies (1:100 diluted in FACS buffer) for
364 flow cytometric analysis. For intracellular staining, cells were cultured in RPMI1640 (ThermoFisher
365 Scientific #11875093) supplemented with 10% FBS, 1% penicillin/streptomycin (ThermoFisher
366 Scientific #15140122) and 1% GlutaMAX (ThermoFisher Scientific #35050061), 1 µL/mL Brefeldin A
367 (BD Biosciences #555029), 50 ng/mL phorbol 12-myristate 13-acetate (Sigma-Aldrich #P1585) and 1
368 ug/mL ionomycin (Sigma-Aldrich #I0634) for 4 hr. Cells were stained for surface markers and fixed
369 using Cytofix/Cytoperm (BD Biosciences #554714) following the manufacture's protocol, and
370 resuspended in Perm/Wash buffer for intracellular cytokine staining. For intranuclear staining, cells
371 were stained for surface markers, fixed using the Foxp3/Transcription Factor Staining Buffer Kit
372 (ThermoFisher Scientific #00-5523-00) and stained for intranuclear markers. Flow cytometry was
373 performed using a BD Fortessa (BD Biosciences). Data analysis was performed using FlowJo
374 software (BD Biosciences).

375 *Cell lines.* Mouse MC38 cell line was a gift from Ryan O'Connell (University of Utah). B16-F10 cells
376 were a gift from the lab of Matthew A. Williams (University of Utah). MC38 cells were grown in DMEM

377 (ThermoFisher Scientific #11965092) supplemented with 10% FBS, 1% penicillin/streptomycin, 1%
378 MEM-NEAA (ThermoFisher Scientific #11140050) and 1% HEPES-Cl pH 7.3 (ThermoFisher Scientific
379 #15630130). B16-F10 cells were grown in DMEM supplemented with 10% FBS and 1%
380 penicillin/streptomycin. NOD 9495 cells were grown similar to a prior report [50] in DMEM (no glutamine,
381 no sodium pyruvate, ThermoFisher Scientific #11960044) supplemented with 10% FBS
382 (ThermoFisher Scientific #A5256701) 1% penicillin/streptomycin, 1% sodium pyruvate, 1% 100×
383 MEM-NEAA, 1% GlutaMAX (ThermoFisher Scientific #35050061). SupT1 human T lymphoblast cells
384 were grown in RPMI1640 supplemented with 5% FBS, 5% calf serum (Sigma), 1%
385 penicillin/streptomycin and 1% GlutaMAX at 37°C with 5% CO_2.

386 *Tumor cell line engraftment.* All tumor experiments used 6- to 10-week-old C57BL/6 or 6~8-week-old
387 NOD background mice. For injections of B16-F10 and MC38, after trypsinization, cultured tumor cells
388 were resuspended in PBS and 1×10^6 and 5×10^5 tumor cells were *s.c.* injected into the hind flank of
389 mice, respectively. For the injection of NOD 9495 tumor line, after trypsinization, cultured tumor cells
390 were resuspended in PBS and 1.5×10^6 tumor cells were *s.c.* injected into the hind flank of mice as
391 described [50].

392 *Small molecules.* Synthesis of DB1033, DB2232, DB2658, DB2379, DB2559, and DB2385 has been
393 previously reported [85]. All compounds were dissolved in 100% DMSO and stored at 5mM at -80°C for
394 later use. For cell-based assays, stock solutions or DMSO vehicle controls were diluted in culture
395 media. For EMSA, compounds were diluted in 0.6X buffer D [86,87]. For mouse injections, sterile PBS
396 was used to dissolve the compounds.

397 *Generation of SupT1 luciferase reporter cell lines.* Reporter constructs were generated using a
398 modified secreted nano-luciferase vector, pNL2.3 (Promega #N108A), with the hygromycin resistance
399 cassette replaced with puromycin resistance cassette (to generate pNL2.3-Puro). Gene blocks
400 (Integrated DNA Technologies) were synthesized containing 5 canonical Oct1 binding motifs
401 (ATGCAAAT, 5×Oct) or mutant motifs (CAAACTAC, 5×Mut) upstream of a minimal CMV promoter.
402 Gene blocks were subcloned into the multiple cloning site of pNL2.3-Puro using EcoRV and HindIII
403 restriction sites. To generate stable transfectants, human SupT1 cells were electroporated using Neon
404 (ThermoFisher Scientific) with 1 μg of either the pNL2.3-Puro empty-vector (EV), pNL2.3-Puro 5×Oct
405 (5×Oct), or pNL2.3-Puro 5×Mut (5×Mut) construct. Electroporation parameters were: 1700 V, 10
406 milliseconds, ×3 pulses. Electroporated cells were allowed to recover for 2 days, then selected for
407 stable DNA integration and expanded in complete media containing 1 μg/mL puromycin
408 (ThermoFisher Scientific #A1113803) for 2 weeks. Cells were then single cell-cloned by limited dilution
409 in complete media containing 1 μg/mL puromycin.

410 *SupT1 OCA-B activity assays.* 1.0×10^5 5×Oct and 5×Mut reporter cells were seeded into wells of 96-
411 well plates were cultured in 100 μL complete RPMI in complete medium with serially diluted
412 compounds for 18-20 hr. Supernatant was collected and mixed with 1:50 buffer-diluted Nano-Glo
413 luciferase substrate (Cat# N1110, Promega). Luminescence was measured using a Modulus
414 Microplate Multimode Reader (Promega).

415 *In vivo treatment of PD-1 blockade-induced diabetes.* NOD.*Ocab*$^{fl/fl}$ and NOD.*Ocab*$^{fl/fl}$;CD4-Cre mice
416 were *i.p.* administered with α-PD-1 and 15 mg/kg of DB1033 was administered *i.p.* to the mice at day
417 0, 4, 8, 11, and 12. Mice were sacrificed on day 24.

418 *Statistical analyses.* Two-tailed student's t-tests were used to determine all statistical differences. All
419 error bars represent ±standard deviations unless otherwise noted. All error bars tumor size represents
420 ±SEM unless otherwise denoted. For all figures, ns, $p > 0.05$; *, $p \leq 0.05$; **, $p \leq 0.01$; ***, $p \leq 0.001$;
421 ****, $p \leq 0.0001$.

422 *Construction and purification of recombinant Oct1 DNA binding domain Oct1-fusion proteins.* A cDNA
423 for the Oct1 DNA binding domain (comprising POU_S and POU_H subdomains) fused to OCA-$_{B1-44}$ was
424 ordered from IDT and included an N-terminal 6-His, consecutive C-terminal Twinstrep and FLAG tags.
425 the cDNAs were cloned into the pET28a vector (Invitrogen) between the *Nco*I and *Hind*III sites. The
426 plasmids were transformed into Rosetta 2 (DE3) pLysS competent cells (Sigma) using 50 µg/ml
427 kanamycin as a selectable marker. Protein was expressed using 1 mM IPTG (Sigma) at 37°C for
428 three hr. The cells were lysed in buffer containing 20 mM HEPES, pH 7.4 (Sigma), 300 mM NaCl
429 (Sigma), 5% glycerol (Sigma) and 1 mM DTT (ThermoFisher Scientific) containing EDTA-free
430 protease inhibitor cocktail (Sigma) at 2X concentration. Protein was bound to a Histrap column
431 (Cytiva) using the same buffer and eluted with buffer containing 400 mM imidazole (Sigma). The
432 protein was further purified by size exclusion chromatography on a Superdex increase 75 10/300 GL
433 column (Cytiva.inc). The column was loaded using PBS containing 1 mM DTT. The protein was
434 analyzed on 12% SDS-PAGE gel visualized by Coomassie staining.

435 *NanoBRET.* The NanoBRET donor plasmid was made by cloning nLuc in-frame with the N-terminus of
436 full-length human Oct1 between the *Nco*I and *Xba*I restriction sites of pACE-MAM2 (Geneva Biotech).
437 The acceptor plasmid was made by cloning full-length human OCA-B containing a C-terminal HaloTag
438 into pHTC vector (Promega) between the *Eco*RI and *Xho*I sites. nanoBRET was performed using the
439 NanoBRET protein:protein interaction kit (Promega) following the manufacturer protocol. Briefly, 2×10^6
440 293T cells were plated in 6-well plates were transfected with a total of 2 µg of donor plus acceptor
441 plasmid at a ratio of 1:100. After 24 hr, cells were harvested and counted. 2×10^5 resuspended cells
442 were seeded into the wells of 96-well plates using DMEM lacking phenol red (ThermoFisher Scientific)
443 containing 10% FBS. After 1 hr, DB1033 or DMSO vehicle control were also added at the indicated
444 concentrations in biological triplicate. After 24 hr, the Nanuck substrate and Halo-ligand were added
445 before measuring BRET ratio using plate reader (Spectromax iD5, Molecular Devices Inc.). The
446 miliBRET ratio was plotted with respect to the DB1033 concentration.

447 *EMSA.* Published protocols [86,87] were used for EMSA. The octamer sequence probe was 5' labeled
448 with Cy-5 and used at a final concentration of 40 nM. The probe was incubated with 10 nM Oct1-OCA
449 B chimeric protein ±equimolar OCA B (1-44) peptide over ice for 15 min prior to the addition of 100
450 nM-400 nM DB1033, then further incubated over ice for another 15 min. Reaction mixtures were
451 electrophoresed through 6% native polyacrylamide gels. Images were collected using a Molecular
452 Dynamics Typhoon scanner using the Cy-5 fluorescence filter.

453 *NanoDSF.* Tryptophan fluorescence at 330 nm and 350 nm were simultaneously monitored over a
454 temperature range from 25°C to 95°C using a NanoTemper Technologies nanoDSF instrument with an
455 excitation wavelength of 280 nm based on published procedures [88]. The Oct1-OCA B chimeric protein
456 complexed with double-stranded DNA containing an Oct1-OCA-B binding site was incubated on ice
457 for 15 min. Protein lacking DNA was used as a control. The effect of DB1033 compound or DMSO
458 control on the protein DNA complex were measured by comparing the melting point of the
459 protein/DNA complex ±DB1033 compound. 10 µl from each sample was loaded into each capillary
460 avoiding any air bubbles. The fluorescence intensity ratio and its first derivative were calculated with

461 the manufacturer's software (PR.ThermControl, version 2.1.2). The smoothened curves and the first
462 derivative were plotted in using Microsoft Excel software. The peak from the first-order derivative
463 indicates the melting temperature of the sample protein sample.

464 **Figure Legends**

465 **Figure 1. OCA-B deletion in T cells confers protection against PD-1 blockade-induced diabetes**
466 **in NOD mice. (A)** Kaplan-Meier plot of diabetes-free mice in 8-week-old male *Ocab*$^{fl/fl}$ (n=7) and
467 *Ocab*$^{fl/fl}$;CD4-Cre (n=7) NOD mice. 250 μg α-PD-1 was administered by intraperitoneal (*i.p.*) injection
468 at day 0, 4, 8 and 12. Blood glucose levels were measured during different stages of diabetes
469 development. **(B)** Blood glucose levels of individual mice from (A). **(C)** Islets were prepared from 8-
470 week-old treated female knockout and littermate control mice 5 days after one dose of α-PD-1
471 antibody and used in flow cytometry. Representative flow cytometry plots depicting total infiltrating
472 CD45$^+$ leukocytes for control and knockout mice. (**D**) Quantification of total infiltrating CD45$^+$ islet
473 leukocyte flow cytometry data from NOD.*Ocab*$^{fl/fl}$ (n=4) and NOD.*Ocab*$^{fl/fl}$;CD4-Cre mice (n=3). (**E**)
474 Representative flow cytometry plots depicting CD4$^+$ and CD8$^+$ islet T cells. Cells were pre-gated using
475 α-CD3 staining. (**F**) Quantification of flow cytometry data showing the percentages of CD4$^+$ and CD8$^+$
476 T cells in islets from NOD.*Ocab*$^{fl/fl}$ (n=4) and NOD.*Ocab*$^{fl/fl}$;CD4-Cre mice (n=3). (**G**) Representative
477 flow cytometry plots showing the percentage of PD-1$^+$SLAMF6$^+$CD39$^-$CD8$^+$ T_{PEX} and PD-1$^+$SLAMF6$^-$
478 CD39$^+$CD8$^+$ T_{EX} in islets (pre-gated on PD-1$^+$CD8$^+$ T cells). (**H**) Quantification of flow cytometry data
479 for the percentage of T_{PEX} and T_{EX} in islets from NOD.*Ocab*$^{fl/fl}$ (n=4) and NOD.*Ocab*$^{fl/fl}$;CD4-Cre mice
480 (n=3).

481

482 **Figure 2. OCA-B in T cells is dispensable for anti-tumor immunity in C57BL/6 mice. (A)** 5×10^5
483 MC38 tumor cells were *s.c.* implanted into the hind flanks of female C57BL/6 *Ocab*$^{fl/fl}$ and
484 *Ocab*$^{fl/fl}$;CD4-Cre mice. 300 μg α-PD-1 (or PBS) was administered *i.p.* at day 4, 7, 10. Tumor sizes
485 were measured every 3-4 days, and mice were euthanized at end point (day 23) or upon tumor size
486 reaching 2 cm in any direction. *Ocab*$^{fl/fl}$+PBS (n=8), *Ocab*$^{fl/fl}$;CD4-Cre+PBS (n=11), *Ocab*$^{fl/fl}$+α-PD-1
487 (n=8), and *Ocab*$^{fl/fl}$;CD4-Cre+α-PD-1 (n=8). **(B)** Mean tumor sizes from (A) are shown. *Ocab*$^{fl/fl}$+PBS
488 (n=8), *Ocab*$^{fl/fl}$;CD4-Cre+PBS (n=11), *Ocab*$^{fl/fl}$+α-PD-1 (n=8), and *Ocab*$^{fl/fl}$;CD4-Cre+α-PD-1 (n=8). **(C)**
489 Quantification of flow cytometry data showing the percentage of CD45.2$^+$ tumor-infiltrating leukocytes
490 (TILs) in MC38 TMEs from α-PD-1 antibody-treated *Ocab*$^{fl/fl}$ (n=6) and *Ocab*$^{fl/fl}$;CD4-Cre (n=6) mice on
491 day 23 or upon tumor size reaching 2 cm in any direction. **(D)** Quantification of flow cytometry data
492 showing the ratio of CD8$^+$ to CD4$^+$ T cells in the TME. **(E)** Representative flow cytometry plots of
493 endpoint TME CD4$^+$ and CD8$^+$ T cell SLAMF6 and CD39 expression. *Ocab*$^{fl/fl}$ (n=6) and *Ocab*$^{fl/fl}$;CD4-
494 Cre (n=5) tumor-bearing mice were treated with α-PD-1 antibodies. (**F**) Quantification of flow
495 cytometry data for endpoint TME CD4$^+$ and CD8$^+$ T cell SLAMF6 and CD39 expression from *Ocab*$^{fl/fl}$
496 (n=6) and *Ocab*$^{fl/fl}$;CD4-Cre (n=5) mice. (**G**) Representative flow cytometry data for endpoint TME
497 CD8$^+$ and CD4$^+$ T cell TIM-3 expression. (**H**) Quantification of flow cytometry data at endpoint showing
498 TME CD4$^+$ and CD8$^+$ T cell TIM-3 expression from *Ocab*$^{fl/fl}$ (n=6) and *Ocab*$^{fl/fl}$;CD4-Cre (n=6) mice.

499

500 **Figure 3. OCA-B in T cells is dispensable for anti-tumor immunity in NOD mice. (A)** 1.5×10^6
501 9495 tumor cells were *s.c.* implanted into the hind flanks of male NOD.*Ocab*$^{fl/fl}$ and NOD.*Ocab*$^{fl/fl}$;CD4-
502 Cre mice. Three doses of 200 μg α-PD-1 (or PBS vehicle control) were *i.p.* administered at day 10, 14
503 and 18. Tumor sizes were measured during different stages of tumor growth. *Ocab*$^{fl/fl}$+PBS (n=3),
504 *Ocab*$^{fl/fl}$;CD4-Cre+PBS (n=4), *Ocab*$^{fl/fl}$+α-PD-1 (n=8), and *Ocab*$^{fl/fl}$;CD4-Cre+α-PD-1 (n=12). **(B)**
505 Quantification of flow cytometry data for the percentage of CD45$^+$ infiltrating cells in the TME from α-
506 PD-1 antibody-treated control *Ocab*$^{fl/fl}$ (n=10) and littermate experimental *Ocab*$^{fl/fl}$;CD4-Cre (n=6) mice.

(C) Representative flow cytometry plots depicting $CD4^+$ and $CD8^+$ TME T cells from α-PD-1 antibody-treated control NOD.*Ocab*$^{fl/fl}$ and littermate experimental NOD.*Ocab*$^{fl/fl}$;CD4-Cre mice. Cells were pre-gated using α-CD3 staining. (**D**) Quantification of flow cytometry data depicting the percentage of $CD4^+$ and $CD8^+$ T cells in the TME from NOD.*Ocab*$^{fl/fl}$ (n=9) and NOD.*Ocab*$^{fl/fl}$;CD4-Cre mice (n=4). (**E**) Quantification of flow cytometry data showing the percentage of activated ($CD62L^{lo}CD44^{hi}$) $CD8^+$ T cells in the TME of α-PD-1-treated *Ocab*$^{fl/fl}$ (n=9) and littermate experimental *Ocab*$^{fl/fl}$;CD4-Cre (n=5) mice at endpoint. (**F**) Representative flow cytometry plots depicting relative percentages of SLAMF6- and CD39-expressing infiltrating $CD8^+PD\text{-}1^+$ T cells. (**G**) Quantification of $PD\text{-}1^+SLAMF6^+CD39^-CD8^+$ T_{PEX} and $PD\text{-}1^+SLAMF6^-CD39^+CD8^+$ T_{EX} in the TME from NOD.*Ocab*$^{fl/fl}$ (n=9) and NOD.*Ocab*$^{fl/fl}$;CD4-Cre mice (n=5). (**H**) Representative flow cytometry plots depicting TIM-3 levels in infiltrating $CD8^+$ T cells. (**I**) Quantification of TIM-3^+ cells in the TME from NOD.*Ocab*$^{fl/fl}$ (n=9) and NOD.*Ocab*$^{fl/fl}$;CD4-Cre mice (n=5).

Figure 4. OCA-B cellular inhibition by small molecule DNA minor groove binders (**A**) Oct1:OCA-B:DNA co-crystal structure [43] showing two targeting approaches: a peptide that mimics the key OCA-B alpha helix involved in downstream effector functions (top lightning bolt) [40], and a minor groove DNA binding molecule with potential to disrupt the unstructured Oct1 linker domain between the two DNA binding subdomains (bottom lightning bolt). (**B**) OCA-B immunoblots from SupT1 and Jurkat T cell lines (lanes 3-4). Isolated mouse primary thymocyte and 293T cell lysates were also used as positive and negative controls, respectively (lanes 1-2). Histone H3 is shown as a loading control. (**C**) Schematic for OCA-B luciferase reporter cell lines. SupT1 cells were stably transfected with reporter plasmids containing five tandem canonical Oct1:OCA-B binding sites linked to a CMV promoter upstream of secreted nLuc (5×Oct) or an identical plasmid except containing mutant binding sites used to determine nonspecific effects (5×Mut). Cells were selected with puromycin, single-cell cloned, and individual clones used subsequently. (**D**) Luciferase activity of pNL2.3 empty vector ("EV"), 5×Oct, or 5×Mut reporter lines. Cells were incubated for 18 hr after plating. (**E**) Luciferase expression kinetics of cultured 5×Oct cells. A timecourse of 2-46 hr is shown. Averages are shown from n=5 biological replicate platings. Trendline shows logistic growth fit. (**F**) Inhibition of cellular OCA-B activity by an escalating dose of the small molecule DB1033. Values from 5×Oct and 5×Mut clones were normalized to one another in the absence of DB1033. Averages are shown across n=6 biological replicate platings. Red curve shows the "5×Oct" fit to the Hill equation. Asterisks denote results from two-tailed student T-test comparing the two lines at the highest concentration. (**G**) Chemical structure of DB1033. (**H**) Molecular docking of DB1033 to canonical octamer B-form DNA. Red shows water molecules. DB1033 is shown in purple. Red/underlined nucleotides show the minor groove bases contacted by DB1033 docked with the lowest free energy. (**I**) Wireframe model showing DB1033 bound to the minor groove AAAT site. Hydrogen bond interactions formed between DB1033 and the minor groove AAAT site are shown with dashed lines.

Figure 5. DB1033 inhibits OCA-B-Oct1-DNA complex formation. (**A**) Schematics of full-length Oct1 tagged with N-terminal nLuc and full-length OCA-B with a C-terminal HaloTag used for nanoBRET. (**B**) Quantification of nanoBRET signal obtained by co-transfecting the 293T cells with the constructs shown in A in the presence of increasing concentrations of DB1033. An average of n=3 biological replicate platings is shown. DB1033 was applied at the indicated concentrations 1 hr after seeding the cells and cells were collected after a further 24 hr.(**C**) Schematics of the C-terminally

Twinstep-tagged Oct1 DNA-binding domain ($Oct1_{DBD}$) and full-length OCA-B with a C-terminal FLAG tag used in EMSA. (**D**) Cy5-DNA scan of native PAGE EMSA showing DNA-$Oct1_{DBD}$ complex formation with OCA-B, and concentration-dependent inhibition by DB1033. (**E**) A schematic of the $Oct1_{DBD}$:OCA-B_{1-44} fusion protein engineered for nanoDSF. (**F**) Structure of the OCA-B_{1-44}-$Oct1_{DBD}$ complex predicted using Alphafold 3. Cyan: OCA-B_{1-44} peptide. Green: $Oct1_{DBD}$ peptide. Dark blue shows the Oct1:DNA structure derived from X-ray crystallography [43]. (**G**) nanoDSF measurement of the thermal stability of 10 μM $Oct1_{DBD}$-OCA-B_{1-44} chimeric protein with or without added canonical octamer DNA. First derivative is shown below. (**H**) First derivative nanoDSF data in the presence of DNA and the presence (above) or absence (below) of 100 μM DB1033.

Figure 6. DB1033 inhibits PD-1 blockade-induced diabetes in NOD mice. (**A**) Kaplan-Meier plot of diabetes-free mice in 8-week-old male NOD.*Ocab*$^{fl/fl}$ treated with PBS (n=4), NOD.*Ocab*$^{fl/fl}$ treated with DB1033 (n=4) and NOD.*Ocab*$^{fl/fl}$;CD4-Cre mice treated with PBS (n=4). Black arrows: 250 µg α-PD-1 and 15 mg/kg *i.p.* injections at day 0, 4, 8, 12. Grey arrow: an additional *i.p.* injection of 15 mg/kg DB1033 was administered on day 11. (**B**) Average blood glucose levels of mice in (A). (**C**) Mouse body weight on day 24 of the experiment described in (A). (**D**) Example H&E images of lacrimal and salivary gland sections harvested from 8-week-old male NOD mice injected with α-PD-1 antibodies in (A). (**E**) Quantification of the histological scoring described in (D). NOD.*Ocab*$^{fl/fl}$ treated with PBS (n=4), NOD.*Ocab*$^{fl/fl}$ treated with DB1033 (n=4) and NOD.*Ocab*$^{fl/fl}$;CD4-Cre mice treated with PBS (n=4). Histologic scoring was conducted in a blinded fashion.

Supplemental Figure Legends

Figure S1. OCA-B deletion in T cells protects NOD mice from spontaneous and PD-1 blockade-induced diabetes. (**A**) Kaplan-Meier plot of diabetes-free mice in 12-week-old female littermate control NOD.*Ocab*$^{fl/fl}$ (n=5) or experimental NOD.*Ocab*$^{fl/fl}$;CD4-Cre (n=6) mice receiving 250 µg α-PD-1 antibody injections at day 0, 4, 8, 12, and 16. Spontaneous T1D was monitored in NOD.*Ocab*$^{fl/fl}$ (n=5) and NOD.*Ocab*$^{fl/fl}$;CD4-Cre (n=5) mice receiving PBS. (**B**) Blood glucose levels were plotted from individual mice receiving α-PD-1 antibody in (A). (**C**) Flow cytometry plots showing percentages of $CD8^+PD\text{-}1^+TIM\text{-}3^+$ islet T cells collected from 12-week-old mice 3 days post-α-PD-1 treatment. (**D**) Quantification of the flow cytometry data from *Ocab*$^{fl/fl}$ (n=4) and *Ocab*$^{fl/fl}$;CD4-Cre mice (n=3). (**E**) 12 week-old NOD.*Ocab*$^{fl/fl}$ or *Ocab*$^{fl/fl}$;CD4-Cre mice were injected once with α-PD-1 antibodies. Islet $CD8^+$ T cells were assessed for SLAMF6 and CD39 by flow cytometry. An example *Ocab*$^{fl/fl}$ and example *Ocab*$^{fl/fl}$;CD4-Cre mouse are shown. (**F**) Quantification of flow cytometry data from *Ocab*$^{fl/fl}$ (n=4) and *Ocab*$^{fl/fl}$;CD4-Cre mice (n=3).

Figure S2. OCA-B deletion in T cells leaves B16F10 tumor growth and immune response unaltered. Growth of *s.c.* B16F10 tumors in C57BL/6 mice sufficient (blue, *Ocab*$^{fl/fl}$) and deficient (red, *Ocab*$^{fl/fl}$;CD4-Cre) for OCA-B in T cells.

Figure S3. OCA-B deletion in T cells decreases the T_{CM}- and naïve-like $CD4^+$ and $CD8^+$ T cell populations in MC38 TME. (A) Representative plots of flow cytometric analysis performed on tumors

592 harvested from 6-10-week-old female α-PD-1-treated C57BL/6.*Ocab*$^{fl/fl}$ and C57BL/6.*Ocab*$^{fl/fl}$;CD4-Cre
593 mice on day 23 post-tumor inoculation (or upon tumor size reaching 2 cm in any direction). CD4$^+$ and
594 CD8$^+$ T_{CM}-like (CD62L$^+$CD44$^+$) and T_N-like (CD62L$^+$CD44$^-$) cells in the TME are shown. (**B**)
595 Quantification of the percentages of T_{CM}-like (CD62L$^+$CD44$^+$) and T_N-like (CD62L$^+$CD44$^-$) in TME
596 CD4$^+$ cells (n=5 *Ocab*$^{fl/fl}$ and n=5 *Ocab*$^{fl/fl}$;CD4-Cre) and CD8$^+$ cells from *Ocab*$^{fl/fl}$ controls and
597 *Ocab*$^{fl/fl}$;CD4-Cre (n=5 *Ocab*$^{fl/fl}$ and n=5 *Ocab*$^{fl/fl}$;CD4-Cre for T_N-like and n=5 *Ocab*$^{fl/fl}$ and n=6
598 *Ocab*$^{fl/fl}$;CD4-Cre for T_{CM}-like).

599

600 **Figure S4. NOD tumor additional data. (A)** Kaplan-Meier plot of another cohort of diabetes-free
601 mice performed with the same experiment procedures as in Figure 3. **(B-C)** Average blood glucose
602 levels of mice in panel A.

603

604 **Figure S5. Effect of staurosporine on luciferase-based transcription activity in SupT1 cells.** A
605 dose curve of staurosporine is shown using both the 5×Oct and 5×Mut cell lines. Trendlines show the
606 fit to the Hill equation.

607

608 **Figure S6. OCA-B cellular inhibition by additional small molecule DNA minor groove binders.**
609 (**A**) Inhibition of cellular OCA-B activity by DB2232. Blue datapoints represent control measurements
610 of nonspecific transcription measured in 5×Mut cells. Red datapoints represent experimental
611 measurements from the 5×Oct line. Luciferase values from both cells lines in were normalized to 1.0
612 in the absence of DB2232. Trendlines show the fit to the Hill equation. (**B-H**) Similar data for additional
613 molecules, except cytotoxicity was measured using AlamarBlue.

614

615 **Figure S7. DB1033 and DB2232 effect on PD-1 blockade-induced diabetes in NOD mice. (A)**
616 Image of a 12% SDS-polyacrylamide gel loaded with the purified recombinant chimeric Oct1 DBD-
617 OCA-B protein and stained with Coomassie blue. Molecular weight makers are shown at left as a
618 standard. **(B)** Size exclusion chromatography elution profile using the Oct1-OCA-B chimera. **(C)**
619 EMSA using the Oct1-OCA-B chimera and Cy5-labeled prefer octamer consensus DNA. **(D)** Kaplan-
620 Meier plot of diabetes-free mice in 8-week-old male NOD.*Ocab*$^{fl/fl}$ mice treated with PBS (n=7),
621 NOD.*Ocab*$^{fl/fl}$ mice treated with DB2232 (n=4) and NOD.*Ocab*$^{fl/fl}$;CD4-Cre mice treated with PBS
622 (n=7). Black arrows: 250 µg α-PD-1 and 15 mg/kg *i.p.* injections at day 0, 4, 8, 12. Grey arrow: an
623 additional *i.p.* injection of 15 mg/kg DB2232 was administered on day 11. **(E)** Average blood glucose
624 levels of mice in (D). **(F)** Body weight of mice at day 24 of the experiment described in (D).

Acknowledgements

We thank R. O'Connell and M. Williams for MC38 and B16F10 cells, and A. Young for the 9495 cells. We thank O. Allen, B. Dalley and the University of Utah High-Throughput Genomics Core facility. We thank J. Marvin and the University of Utah Flow Cytometry Core facility. We acknowledge the Huntsman Cancer Institute Cancer Center Support Grant (CCSG). This work was supported by grants from the National Institutes of Health/National Institute of Allergy and Infectious Diseases (R01AI162929), the Praespero Autoimmune Fund (Canada), and an internal seed grant from the Huntsman Cancer Institute Genomics, Epigenetics and Metabolism (GEM) program to DT.

Author contributions

JD, AKM, EPH and PB performed experiments and analyzed data. AY provided key reagents and methods. WDW and AAF synthesized and purified DNA minor groove binding small molecules. DT conceptualized and supervised the study. All authors contributed to the writing of the manuscript.

References

1. National Diabetes Statistics Report. (2024). Centers for Disease Control and Prevention.
2. Ogrotis, I., Koufakis, T., and Kotsa, K. (2023). Changes in the Global Epidemiology of Type 1 Diabetes in an Evolving Landscape of Environmental Factors: Causes, Challenges, and Opportunities. Medicina (Kaunas) *59*. 10.3390/medicina59040668.
3. Gregory, G.A., Robinson, T.I.G., Linklater, S.E., Wang, F., Colagiuri, S., de Beaufort, C., Donaghue, K.C., Magliano, D.J., Maniam, J., Orchard, T.J., et al. (2022). Global incidence, prevalence, and mortality of type 1 diabetes in 2021 with projection to 2040: a modelling study. Lancet Diabetes Endocrinol *10*, 741-760. 10.1016/S2213-8587(22)00218-2.
4. Cooke, D.W., and Plotnick, L. (2008). Type 1 diabetes mellitus in pediatrics. Pediatr Rev *29*, 374-384; quiz 385.
5. Sutherland, D.E., Sibley, R., Xu, X.Z., Michael, A., Srikanta, A.M., Taub, F., Najarian, J., and Goetz, F.C. (1984). Twin-to-twin pancreas transplantation: reversal and reenactment of the pathogenesis of type I diabetes. Trans Assoc Am Physicians *97*, 80-87.
6. Vendrame, F., Pileggi, A., Laughlin, E., Allende, G., Martin-Pagola, A., Molano, R.D., Diamantopoulos, S., Standifer, N., Geubtner, K., Falk, B.A., et al. (2010). Recurrence of type 1 diabetes after simultaneous pancreas-kidney transplantation, despite immunosuppression, is associated with autoantibodies and pathogenic autoreactive CD4 T-cells. Diabetes *59*, 947-957. 10.2337/db09-0498.
7. Wang, Y., Pontesilli, O., Gill, R.G., La Rosa, F.G., and Lafferty, K.J. (1991). The role of CD4+ and CD8+ T cells in the destruction of islet grafts by spontaneously diabetic mice. Proc Natl Acad Sci U S A *88*, 527-531. 10.1073/pnas.88.2.527.
8. Lernmark, A., and Larsson, H.E. (2013). Immune therapy in type 1 diabetes mellitus. Nat Rev Endocrinol *9*, 92-103.
9. Tawbi, H.A., Schadendorf, D., Lipson, E.J., Ascierto, P.A., Matamala, L., Castillo Gutierrez, E., Rutkowski, P., Gogas, H.J., Lao, C.D., De Menezes, J.J., et al. (2022). Relatlimab and Nivolumab versus Nivolumab in Untreated Advanced Melanoma. N Engl J Med *386*, 24-34. 10.1056/NEJMoa2109970.
10. Hamid, O., Robert, C., Daud, A., Hodi, F.S., Hwu, W.J., Kefford, R., Wolchok, J.D., Hersey, P., Joseph, R.W., Weber, J.S., et al. (2013). Safety and tumor responses with lambrolizumab (anti-PD-1) in melanoma. N Engl J Med *369*, 134-144. 10.1056/NEJMoa1305133.
11. Cortes, J., Rugo, H.S., Cescon, D.W., Im, S.A., Yusof, M.M., Gallardo, C., Lipatov, O., Barrios, C.H., Perez-Garcia, J., Iwata, H., et al. (2022). Pembrolizumab plus Chemotherapy in Advanced Triple-Negative Breast Cancer. N Engl J Med *387*, 217-226. 10.1056/NEJMoa2202809.
12. Postow, M.A., Callahan, M.K., and Wolchok, J.D. (2015). Immune Checkpoint Blockade in Cancer Therapy. J Clin Oncol *33*, 1974-1982. 10.1200/JCO.2014.59.4358.
13. Berti, A., Bortolotti, R., Dipasquale, M., Kinspergher, S., Prokop, L., Grandi, G., Inchiostro, S., Paolazzi, G., Caffo, O., and Veccia, A. (2021). Meta-analysis of immune-related adverse events in phase 3 clinical trials assessing immune checkpoint inhibitors for lung cancer. Crit Rev Oncol Hematol *162*, 103351. 10.1016/j.critrevonc.2021.103351.
14. Chen, T.W., Razak, A.R., Bedard, P.L., Siu, L.L., and Hansen, A.R. (2015). A systematic review of immune-related adverse event reporting in clinical trials of immune checkpoint inhibitors. Ann Oncol *26*, 1824-1829. 10.1093/annonc/mdv182.
15. Postow, M.A., Sidlow, R., and Hellmann, M.D. (2018). Immune-Related Adverse Events Associated with Immune Checkpoint Blockade. N Engl J Med *378*, 158-168. 10.1056/NEJMra1703481.
16. Young, A., Quandt, Z., and Bluestone, J.A. (2018). The Balancing Act between Cancer Immunity and Autoimmunity in Response to Immunotherapy. Cancer Immunol Res *6*, 1445-1452. 10.1158/2326-6066.CIR-18-0487.
17. Molina, G.E., Zubiri, L., Cohen, J.V., Durbin, S.M., Petrillo, L., Allen, I.M., Murciano-Goroff, Y.R., Dougan, M., Thomas, M.F., Faje, A.T., et al. (2021). Temporal Trends and Outcomes

Among Patients Admitted for Immune-Related Adverse Events: A Single-Center Retrospective Cohort Study from 2011 to 2018. Oncologist *26*, 514-522. 10.1002/onco.13740.

18. Stamatouli, A.M., Quandt, Z., Perdigoto, A.L., Clark, P.L., Kluger, H., Weiss, S.A., Gettinger, S., Sznol, M., Young, A., Rushakoff, R., et al. (2018). Collateral Damage: Insulin-Dependent Diabetes Induced With Checkpoint Inhibitors. Diabetes *67*, 1471-1480. 10.2337/dbi18-0002.

19. Quandt, Z., Young, A., Perdigoto, A.L., Herold, K.C., and Anderson, M.S. (2021). Autoimmune Endocrinopathies: An Emerging Complication of Immune Checkpoint Inhibitors. Annu Rev Med *72*, 313-330. 10.1146/annurev-med-050219-034237.

20. Osorio, J.C., Ni, A., Chaft, J.E., Pollina, R., Kasler, M.K., Stephens, D., Rodriguez, C., Cambridge, L., Rizvi, H., Wolchok, J.D., et al. (2017). Antibody-mediated thyroid dysfunction during T-cell checkpoint blockade in patients with non-small-cell lung cancer. Ann Oncol *28*, 583-589. 10.1093/annonc/mdw640.

21. Noble, J.A., and Valdes, A.M. (2011). Genetics of the HLA region in the prediction of type 1 diabetes. Curr Diab Rep *11*, 533-542. 10.1007/s11892-011-0223-x.

22. Hu, H., Zakharov, P.N., Peterson, O.J., and Unanue, E.R. (2020). Cytocidal macrophages in symbiosis with CD4 and CD8 T cells cause acute diabetes following checkpoint blockade of PD-1 in NOD mice. Proc Natl Acad Sci U S A *117*, 31319-31330. 10.1073/pnas.2019743117.

23. Sims, E.K., Bundy, B.N., Stier, K., Serti, E., Lim, N., Long, S.A., Geyer, S.M., Moran, A., Greenbaum, C.J., Evans-Molina, C., et al. (2021). Teplizumab improves and stabilizes beta cell function in antibody-positive high-risk individuals. Sci Transl Med *13*. 10.1126/scitranslmed.abc8980.

24. Ramos, E.L., Dayan, C.M., Chatenoud, L., Sumnik, Z., Simmons, K.M., Szypowska, A., Gitelman, S.E., Knecht, L.A., Niemoeller, E., Tian, W., et al. (2023). Teplizumab and beta-Cell Function in Newly Diagnosed Type 1 Diabetes. N Engl J Med *389*, 2151-2161. 10.1056/NEJMoa2308743.

25. Zwilling, S., Dieckmann, A., Pfisterer, P., Angel, P., and Wirth, T. (1997). Inducible expression and phosphorylation of coactivator BOB.1/OBF.1 in T cells. Science *277*, 221-225.

26. Sun, W., Hughes, E.P., Kim, H., Perovanovic, J., Charley, K.R., Perkins, B., Du, J., Ibarra, A., Syage, A.R., Hale, J.S., et al. (2024). OCA-B/Pou2af1 is sufficient to promote CD4+ T cell memory and prospectively identifies memory precursors. Proc Natl Acad Sci U S A *121*, e2309153121. 10.1073/pnas.2309153121.

27. Shakya, A., Kang, J., Chumley, J., Williams, M.A., and Tantin, D. (2011). Oct1 is a switchable, bipotential stabilizer of repressed and inducible transcriptional states. J Biol Chem *286*, 450-459. 10.1074/jbc.M110.174045.

28. Shakya, A., Goren, A., Shalek, A., German, C.N., Snook, J., Kuchroo, V.K., Yosef, N., Chan, R.C., Regev, A., Williams, M.A., and Tantin, D. (2015). Oct1 and OCA-B are selectively required for CD4 memory T cell function. J Exp Med *212*, 2115-2131. 10.1084/jem.20150363.

29. Hughes, E.P., Syage, A.R., Mirzaei Mehrabad, E., Lane, T.E., Spike, B.T., and Tantin, D. (2025). OCA-B promotes pathogenic maturation of stem-like CD4+ T cells and autoimmune demyelination. J Clin Invest. 10.1172/JCI187862.

30. Nakamura, M., Nishida, N., Kawashima, M., Aiba, Y., Tanaka, A., Yasunami, M., Nakamura, H., Komori, A., Nakamuta, M., Zeniya, M., et al. (2012). Genome-wide association study identifies TNFSF15 and POU2AF1 as susceptibility loci for primary biliary cirrhosis in the Japanese population. Am J Hum Genet *91*, 721-728.

31. Goris, A., Sawcer, S., Vandenbroeck, K., Carton, H., Billiau, A., Setakis, E., Compston, A., and Dubois, B. (2003). New candidate loci for multiple sclerosis susceptibility revealed by a whole genome association screen in a Belgian population. J Neuroimmunol *143*, 65-69. 10.1016/j.jneuroim.2003.08.013.

32. Ban, M., Booth, D., Heard, R., Stewart, G., Goris, A., Vandenbroeck, K., Dubois, B., Laaksonen, M., Ilonen, J., Alizadeh, M., et al. (2006). Linkage disequilibrium screening for multiple sclerosis implicates JAG1 and POU2AF1 as susceptibility genes in Europeans. J Neuroimmunol *179*, 108-116.

743 33. van Heel, D.A., Udalova, I.A., De Silva, A.P., McGovern, D.P., Kinouchi, Y., Hull, J., Lench,
744 N.J., Cardon, L.R., Carey, A.H., Jewell, D.P., and Kwiatkowski, D. (2002). Inflammatory bowel
745 disease is associated with a TNF polymorphism that affects an interaction between the OCT1
746 and NF(-kappa)B transcription factors. Hum Mol Genet *11*, 1281-1289.
747 34. Cunninghame Graham, D.S., Wong, A.K., McHugh, N.J., Whittaker, J.C., and Vyse, T.J.
748 (2006). Evidence for unique association signals in SLE at the CD28-CTLA4-ICOS locus in a
749 family-based study. Hum Mol Genet *15*, 3195-3205.
750 35. Leon Rodriguez, D.A., Carmona, F.D., Echeverria, L.E., Gonzalez, C.I., and Martin, J. (2016).
751 IL18 Gene Variants Influence the Susceptibility to Chagas Disease. PLoS Negl Trop Dis *10*,
752 e0004583.
753 36. Kiesler, P., Shakya, A., Tantin, D., and Vercelli, D. (2009). An Allergy-Associated Polymorphism
754 in a Novel Regulatory Element Enhances IL13 Expression. Hum Molec Genet *18*, 4513-4520.
755 37. Vince, N., Li, H., Ramsuran, V., Naranbhai, V., Duh, F.M., Fairfax, B.P., Saleh, B., Knight, J.C.,
756 Anderson, S.K., and Carrington, M. (2016). HLA-C Level Is Regulated by a Polymorphic Oct1
757 Binding Site in the HLA-C Promoter Region. Am J Hum Genet *99*, 1353-1358.
758 38. Farh, K.K., Marson, A., Zhu, J., Kleinewietfeld, M., Housley, W.J., Beik, S., Shoresh, N.,
759 Whitton, H., Ryan, R.J., Shishkin, A.A., et al. (2015). Genetic and epigenetic fine mapping of
760 causal autoimmune disease variants. Nature *518*, 337-343.
761 39. Maurano, M.T., Humbert, R., Rynes, E., Thurman, R.E., Haugen, E., Wang, H., Reynolds, A.P.,
762 Sandstrom, R., Qu, H., Brody, J., et al. (2012). Systematic localization of common disease-
763 associated variation in regulatory DNA. Science *337*, 1190-1195. 10.1126/science.1222794.
764 40. Kim, H., Perovanovic, J., Shakya, A., Shen, Z., German, C.N., A., I., Jafek, J.L., Lin, N.-P.,
765 Evavold, B.D., Chou, D.H., et al. (2021). Targeting OCA-B/Pou2af1 blocks activated,
766 autoreactive T cells in the pancreas and type-1 diabetes. J Exp Med *218*, e20200533.
767 10.1084/jem.20200533.
768 41. Strubin, M., Newell, J.W., and Matthias, P. (1995). OBF-1, a novel B cell-specific coactivator
769 that stimulates immunoglobulin promoter activity through association with octamer-binding
770 proteins. Cell *80*, 497-506.
771 42. Gstaiger, M., Knoepfel, L., Georgiev, O., Schaffner, W., and Hovens, C.M. (1995). A B-cell
772 coactivator of octamer-binding transcription factors. Nature *373*, 360-362.
773 43. Chasman, D., Cepek, K., Sharp, P.A., and Pabo, C.O. (1999). Crystal structure of an OCA-B
774 peptide bound to an Oct-1 POU domain/octamer DNA complex: specific recognition of a
775 protein-DNA interface. Genes Dev. *13*, 2650-2657.
776 44. Ansari, M.J., Salama, A.D., Chitnis, T., Smith, R.N., Yagita, H., Akiba, H., Yamazaki, T., Azuma,
777 M., Iwai, H., Khoury, S.J., et al. (2003). The programmed death-1 (PD-1) pathway regulates
778 autoimmune diabetes in nonobese diabetic (NOD) mice. J Exp Med *198*, 63-69.
779 10.1084/jem.20022125.
780 45. Fife, B.T., Guleria, I., Gubbels Bupp, M., Eagar, T.N., Tang, Q., Bour-Jordan, H., Yagita, H.,
781 Azuma, M., Sayegh, M.H., and Bluestone, J.A. (2006). Insulin-induced remission in new-onset
782 NOD mice is maintained by the PD-1-PD-L1 pathway. J Exp Med *203*, 2737-2747.
783 10.1084/jem.20061577.
784 46. Zhou, J., Jin, J.O., Kawai, T., and Yu, Q. (2016). Endogenous programmed death ligand-1
785 restrains the development and onset of Sjögren's syndrome in non-obese diabetic mice. Sci
786 Rep *6*, 39105. 10.1038/srep39105.
787 47. Ippolito, S., Di Dalmazi, G., Pani, F., Sabini, E., and Caturegli, P. (2021). Distinct Cytokine
788 Signatures in Thyroiditis Induced by PD-1 or CTLA-4 Blockade: Insights from a New Mouse
789 Model. Thyroid *31*, 1839-1849. 10.1089/thy.2021.0165.
790 48. Martinez-Usatorre, A., Donda, A., Zehn, D., and Romero, P. (2018). PD-1 Blockade Unleashes
791 Effector Potential of Both High- and Low-Affinity Tumor-Infiltrating T Cells. J Immunol *201*, 792-
792 803. 10.4049/jimmunol.1701644.
793 49. Homet Moreno, B., Zaretsky, J.M., Garcia-Diaz, A., Tsoi, J., Parisi, G., Robert, L., Meeth, K.,
794 Ndoye, A., Bosenberg, M., Weeraratna, A.T., et al. (2016). Response to Programmed Cell

Death-1 Blockade in a Murine Melanoma Syngeneic Model Requires Costimulation, CD4, and CD8 T Cells. Cancer Immunol Res *4*, 845-857. 10.1158/2326-6066.CIR-16-0060.

50. Young, A., Medrano, R., Wynn, P., Kang, J.H., Hansen, C., Cina, M., Fadlullah, M.C.H., Sheehan, K.C.F., Quandt, Z., Nahar, K., et al. (2025). Improving preclinical modeling of irAEs and anti-tumor immunity using syngeneic tumor models in autoimmune-prone NOD mice. in prep.
51. Abramson, J., Adler, J., Dunger, J., Evans, R., Green, T., Pritzel, A., Ronneberger, O., Willmore, L., Ballard, A.J., Bambrick, J., et al. (2024). Accurate structure prediction of biomolecular interactions with AlphaFold 3. Nature *630*, 493-500. 10.1038/s41586-024-07487-w.
52. Wu, X.S., He, X.Y., Ipsaro, J.J., Huang, Y.H., Preall, J.B., Ng, D., Shue, Y.T., Sage, J., Egeblad, M., Joshua-Tor, L., and Vakoc, C.R. (2022). OCA-T1 and OCA-T2 are coactivators of POU2F3 in the tuft cell lineage. Nature *607*, 169-175. 10.1038/s41586-022-04842-7.
53. Betzler, A.C., Fiedler, K., Hoffmann, T.K., Fehling, H.J., Wirth, T., and Brunner, C. (2022). BOB.1/OBF.1 is required during B-cell ontogeny for B-cell differentiation and germinal center function. Eur J Immunol *52*, 404-417. 10.1002/eji.202149333.
54. Shi, W., Liao, Y., Willis, S.N., Taubenheim, N., Inouye, M., Tarlinton, D.M., Smyth, G.K., Hodgkin, P.D., Nutt, S.L., and Corcoran, L.M. (2015). Transcriptional profiling of mouse B cell terminal differentiation defines a signature for antibody-secreting plasma cells. Nat Immunol *16*, 663-673.
55. Kim, U., Qin, X.F., Gong, S., Stevens, S., Luo, Y., Nussensweig, M., and Roeder, R.G. (1996). The B-cell-specific transcription coactivator OCA-B/OBF-1/Bob-1 is essential for normal production of immunoglobulin isotypes. Nature *383*, 542-547.
56. Schubart, D.B., Rolink, A., Kosco-Vilbois, R.G., Botteri, F., and Matthias, P. (1996). B-cell-specific coactivator OBF-1/OCA-B/Bob1 required for immune response and germinal centre formation. Nature *383*, 538-542.
57. Chee, J., Ko, H.J., Skowera, A., Jhala, G., Catterall, T., Graham, K.L., Sutherland, R.M., Thomas, H.E., Lew, A.M., Peakman, M., et al. (2014). Effector-memory T cells develop in islets and report islet pathology in type 1 diabetes. J Immunol *192*, 572-580.
58. Gearty, S.V., Dundar, F., Zumbo, P., Espinosa-Carrasco, G., Shakiba, M., Sanchez-Rivera, F.J., Socci, N.D., Trivedi, P., Lowe, S.W., Lauer, P., et al. (2022). An autoimmune stem-like CD8 T cell population drives type 1 diabetes. Nature *602*, 156-161. 10.1038/s41586-021-04248-x.
59. Li, Y., Ramirez-Suastegui, C., Harris, R., Castaneda-Castro, F.E., Ascui, G., Perez-Jeldres, T., Diaz, A., Morong, C., Giles, D.A., Chai, J., et al. (2024). Stem-like T cells are associated with the pathogenesis of ulcerative colitis in humans. Nat Immunol *25*, 1231-1244. 10.1038/s41590-024-01860-7.
60. Hughes, E.P., Syage, A.R., and Tantin, D. (2024). Durable CD4+ immunity: cherchez la stem. Trends Imm *45*, 158-166. 10.1016/j.it.2024.01.004.
61. Polo, J.M., Dell'Oso, T., Ranuncolo, S.M., Cerchietti, L., Beck, D., Da Silva, G.F., Prive, G.G., Licht, J.D., and Melnick, A. (2004). Specific peptide interference reveals BCL6 transcriptional and oncogenic mechanisms in B-cell lymphoma cells. Nat Med *10*, 1329-1335.
62. Caron, N.J., Quenneville, S.P., and Tremblay, J.P. (2004). Endosome disruption enhances the functional nuclear delivery of Tat-fusion proteins. Biochem Biophys Res Commun *319*, 12-20.
63. Krautwald, S., Ziegler, E., Tiede, K., Pust, R., and Kunzendorf, U. (2004). Transduction of the TAT-FLIP fusion protein results in transient resistance to Fas-induced apoptosis in vivo. J Biol Chem *279*, 44005-44011.
64. Wright, H.M., Clish, C.B., Mikami, T., Hauser, S., Yanagi, K., Hiramatsu, R., Serhan, C.N., and Spiegelman, B.M. (2000). A synthetic antagonist for the peroxisome proliferator-activated receptor gamma inhibits adipocyte differentiation. J Biol Chem *275*, 1873-1877.
65. Vassilev, L.T., Vu, B.T., Graves, B., Carvajal, D., Podlaski, F., Filipovic, Z., Kong, N., Kammlott, U., Lukacs, C., Klein, C., et al. (2004). In vivo activation of the p53 pathway by small-molecule antagonists of MDM2. Science *303*, 844-848. 10.1126/science.1092472.

848 66. Cerchietti, L.C., Yang, S.N., Shaknovich, R., Hatzi, K., Polo, J.M., Chadburn, A., Dowdy, S.F.,
849 and Melnick, A. (2009). A peptomimetic inhibitor of BCL6 with potent antilymphoma effects in
850 vitro and in vivo. Blood *113*, 3397-3405. 10.1182/blood-2008-07-168773.
851 67. Green, D.R. (2016). A BH3 Mimetic for Killing Cancer Cells. Cell *165*, 1560.
852 68. Skwarczynska, M., and Ottmann, C. (2015). Protein-protein interactions as drug targets.
853 Future Med Chem *7*, 2195-2219.
854 69. Lu, G., Middleton, R.E., Sun, H., Naniong, M., Ott, C.J., Mitsiades, C.S., Wong, K.K., Bradner,
855 J.E., and Kaelin, W.G., Jr. (2014). The myeloma drug lenalidomide promotes the cereblon-
856 dependent destruction of Ikaros proteins. Science *343*, 305-309. 10.1126/science.1244917.
857 70. Fischer, E.S., Böhm, K., Lydeard, J.R., Yang, H., Stadler, M.B., Cavadini, S., Nagel, J.,
858 Serluca, F., Acker, V., Lingaraju, G.M., et al. (2014). Structure of the DDB1-CRBN E3 ubiquitin
859 ligase in complex with thalidomide. Nature *512*, 49-53. 10.1038/nature13527.
860 71. Fiskus, W., Mill, C.P., Nabet, B., Perera, D., Birdwell, C., Manshouri, T., Lara, B., Kadia, T.M.,
861 DiNardo, C., Takahashi, K., et al. (2021). Superior efficacy of co-targeting GFI1/KDM1A and
862 BRD4 against AML and post-MPN secondary AML cells. Blood Cancer J *11*, 98.
863 10.1038/s41408-021-00487-3.
864 72. Issa, G.C., Aldoss, I., DiPersio, J., Cuglievan, B., Stone, R., Arellano, M., Thirman, M.J., Patel,
865 M.R., Dickens, D.S., Shenoy, S., et al. (2023). The menin inhibitor revumenib in KMT2A-
866 rearranged or NPM1-mutant leukaemia. Nature *615*, 920-924. 10.1038/s41586-023-05812-3.
867 73. Antony-Debré, I., Paul, A., Leite, J., Mitchell, K., Kim, H.M., Carvajal, L.A., Todorova, T.I.,
868 Huang, K., Kumar, A., Farahat, A.A., et al. (2017). Pharmacological inhibition of the
869 transcription factor PU.1 in leukemia. J Clin Invest *127*, 4297-4313. 10.1172/jci92504.
870 74. Taylor, S.J., Stauber, J., Bohorquez, O., Tatsumi, G., Kumari, R., Chakraborty, J., Bartholdy,
871 B.A., Schwenger, E., Sundaravel, S., Farahat, A.A., et al. (2024). Pharmacological restriction
872 of genomic binding sites redirects PU.1 pioneer transcription factor activity. Nat Genet *56*,
873 2213-2227. 10.1038/s41588-024-01911-7.
874 75. Gibson, S.A., Yang, W., Yan, Z., Qin, H., and Benveniste, E.N. (2018). CK2 Controls Th17 and
875 Regulatory T Cell Differentiation Through Inhibition of FoxO1. J Immunol *201*, 383-392.
876 10.4049/jimmunol.1701592.
877 76. Wang, F., Demir, S., Gehringer, F., Osswald, C.D., Seyfried, F., Enzenmüller, S., Eckhoff, S.M.,
878 Maier, T., Holzmann, K., Debatin, K.M., et al. (2018). Tight regulation of FOXO1 is essential for
879 maintenance of B-cell precursor acute lymphoblastic leukemia. Blood *131*, 2929-2942.
880 10.1182/blood-2017-10-813576.
881 77. Klase, Z., Yedavalli, V.S., Houzet, L., Perkins, M., Maldarelli, F., Brenchley, J., Strebel, K., Liu,
882 P., and Jeang, K.T. (2014). Activation of HIV-1 from latent infection via synergy of RUNX1
883 inhibitor Ro5-3335 and SAHA. PLoS Pathog *10*, e1003997. 10.1371/journal.ppat.1003997.
884 78. Zhu, J., Singh, M., Selivanova, G., and Peuget, S. (2020). Pifithrin-α alters p53 post-
885 translational modifications pattern and differentially inhibits p53 target genes. Sci Rep *10*,
886 1049. 10.1038/s41598-020-58051-1.
887 79. Struntz, N.B., Chen, A., Deutzmann, A., Wilson, R.M., Stefan, E., Evans, H.L., Ramirez, M.A.,
888 Liang, T., Caballero, F., Wildschut, M.H.E., et al. (2019). Stabilization of the Max Homodimer
889 with a Small Molecule Attenuates Myc-Driven Transcription. Cell Chem Biol *26*, 711-723.e714.
890 10.1016/j.chembiol.2019.02.009.
891 80. Frangoul, H., Altshuler, D., Cappellini, M.D., Chen, Y.S., Domm, J., Eustace, B.K., Foell, J., de
892 la Fuente, J., Grupp, S., Handgretinger, R., et al. (2021). CRISPR-Cas9 Gene Editing for
893 Sickle Cell Disease and β-Thalassemia. N Engl J Med *384*, 252-260.
894 10.1056/NEJMoa2031054.
895 81. Jonasch, E., Donskov, F., Iliopoulos, O., Rathmell, W.K., Narayan, V.K., Maughan, B.L.,
896 Oudard, S., Else, T., Maranchie, J.K., Welsh, S.J., et al. (2021). Belzutifan for Renal Cell
897 Carcinoma in von Hippel-Lindau Disease. N Engl J Med *385*, 2036-2046.
898 10.1056/NEJMoa2103425.
899 82. Bushweller, J.H. (2019). Targeting transcription factors in cancer - from undruggable to reality.
900 Nat Rev Cancer *19*, 611-624. 10.1038/s41568-019-0196-7.

83. Bekes, M., Langley, D.R., and Crews, C.M. (2022). PROTAC targeted protein degraders: the past is prologue. Nat Rev Drug Discov *21*, 181-200. 10.1038/s41573-021-00371-6.
84. Jing, Y., Kong, Y., Allard, D., Liu, B., Kolawole, E., Sprouse, M., Evavold, B., Bettini, M., and Bettini, M. (2023). Increased TCR signaling in regulatory T cells is disengaged from TCR affinity. bioRxiv. 10.1101/2023.01.17.523999.
85. Liu, Y., Chai, Y., Kumar, A., Tidwell, R.R., Boykin, D.W., and Wilson, W.D. (2012). Designed compounds for recognition of 10 base pairs of DNA with two at binding sites. J Am Chem Soc *134*, 5290-5299. 10.1021/ja211628j.
86. Tantin, D., Gemberling, M., Callister, C., and Fairbrother, W. (2008). High-throughput Biochemical Analysis of in-vivo Location Data Reveals Novel Distinct Classes of POU5F1(Oct4)/DNA complexes. Genome Res *18*, 631-639.
87. Wang, V.E., Schmidt, T., Chen, J., Sharp, P.A., and Tantin, D. (2004). Embryonic Lethality, Decreased Erythopoiesis, and Defective Octamer-Dependent Promoter Activation in Oct-1-Deficient Mice. Mol Cell Biol *24*, 1022-1032.
88. Magnusson, A.O., Szekrenyi, A., Joosten, H.J., Finnigan, J., Charnock, S., and Fessner, W.D. (2019). nanoDSF as screening tool for enzyme libraries and biotechnology development. FEBS J *286*, 184-204. 10.1111/febs.14696.

Du et al. Figure 1

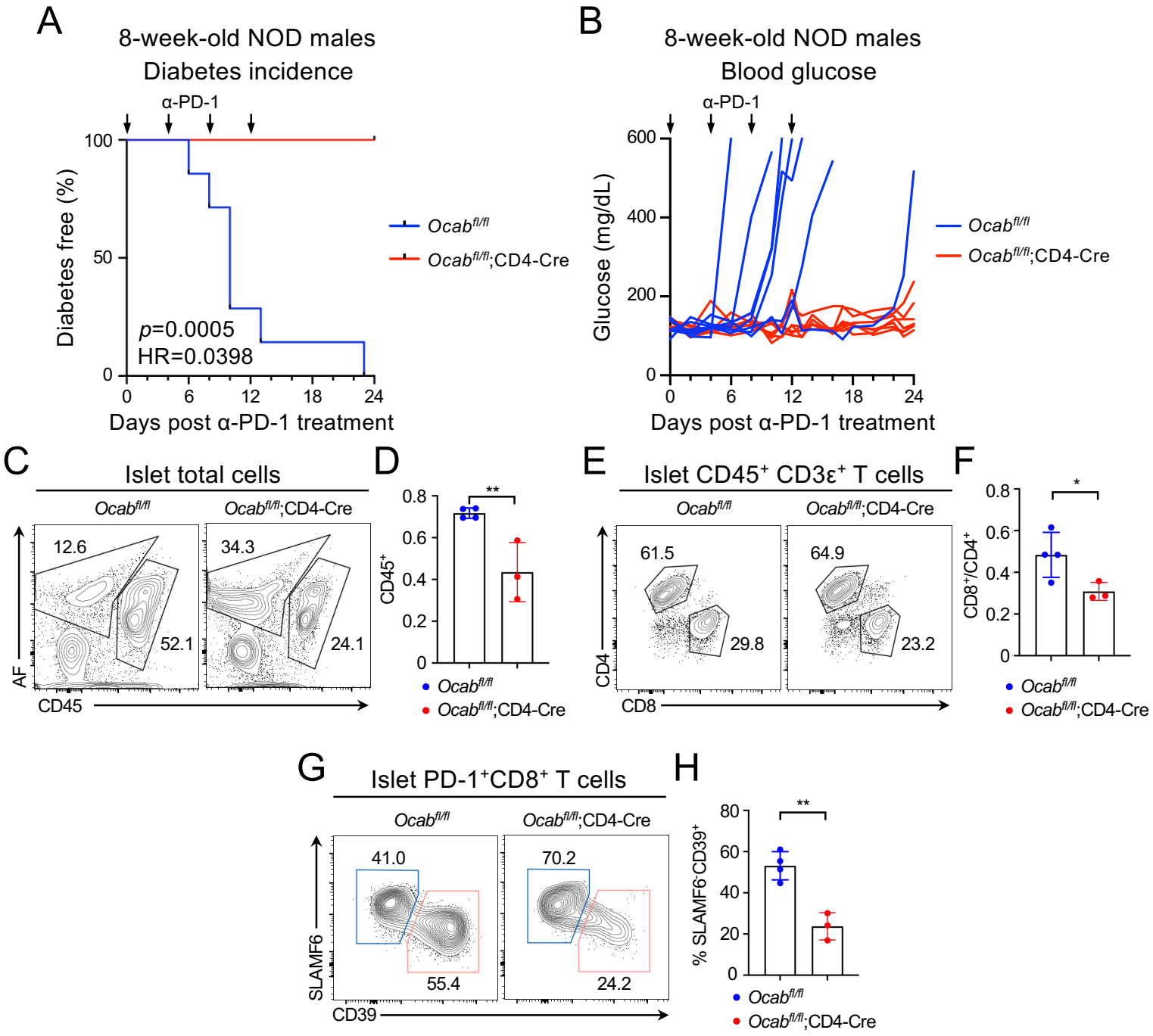

Du et al. Figure 2

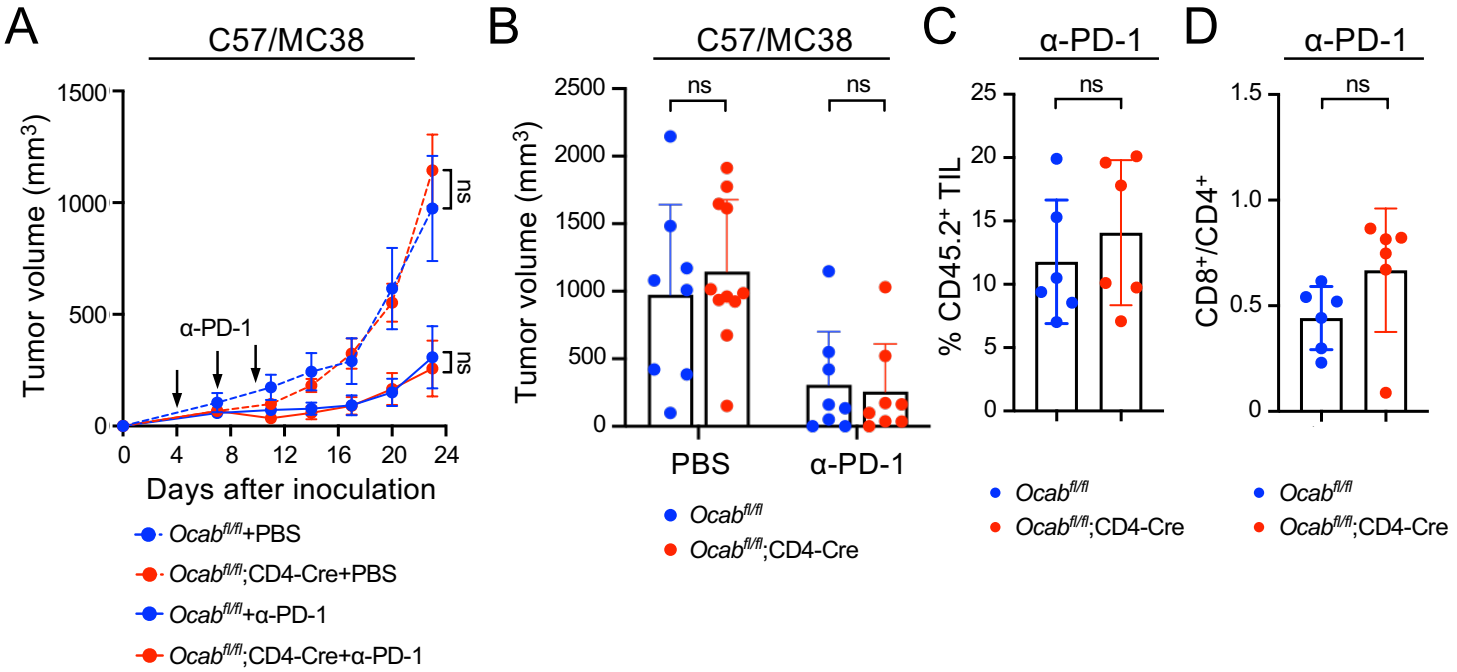

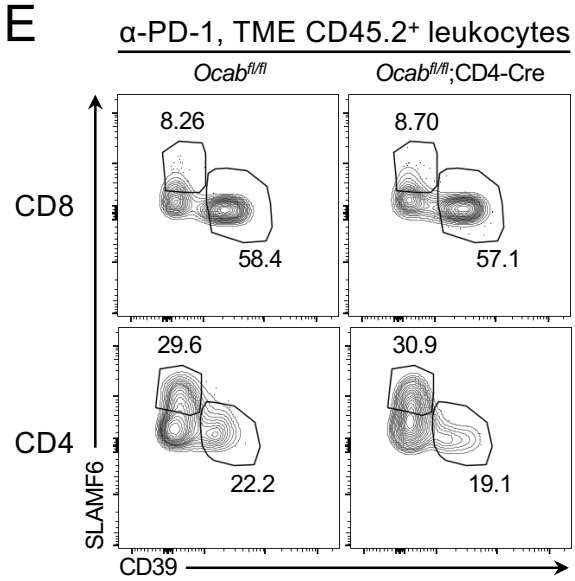

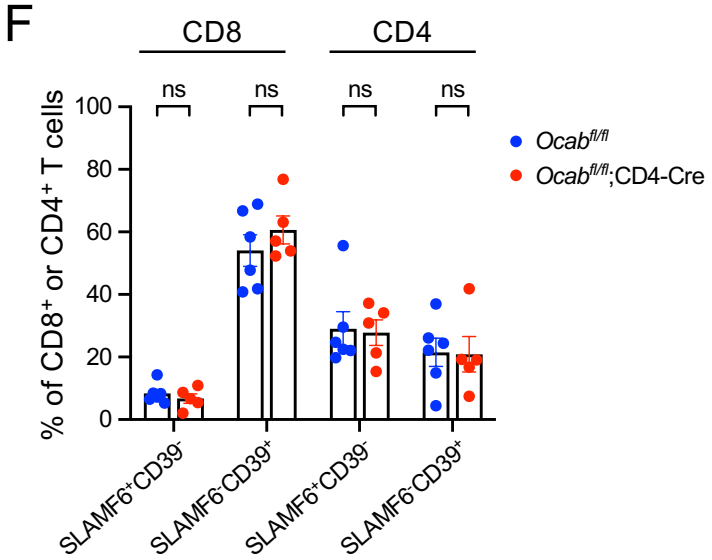

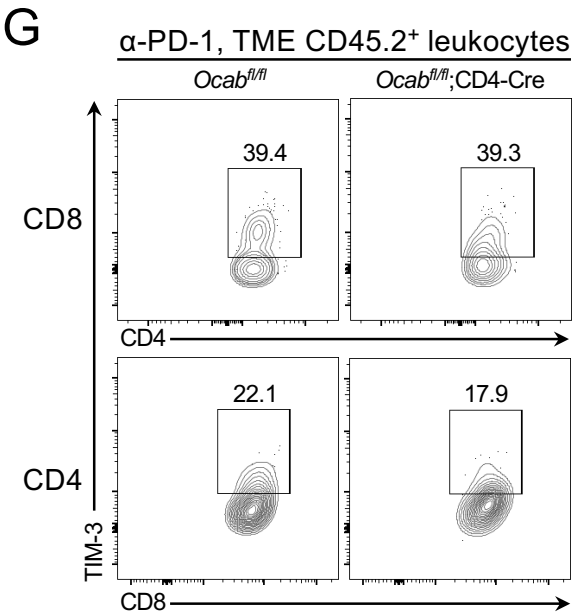

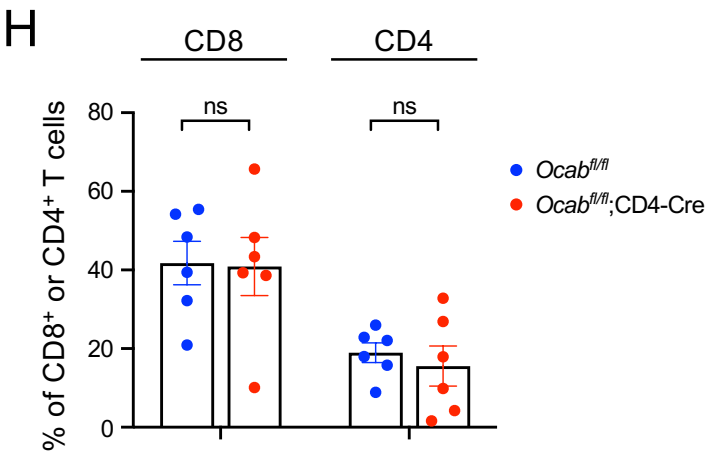

Du et al. Figure 3

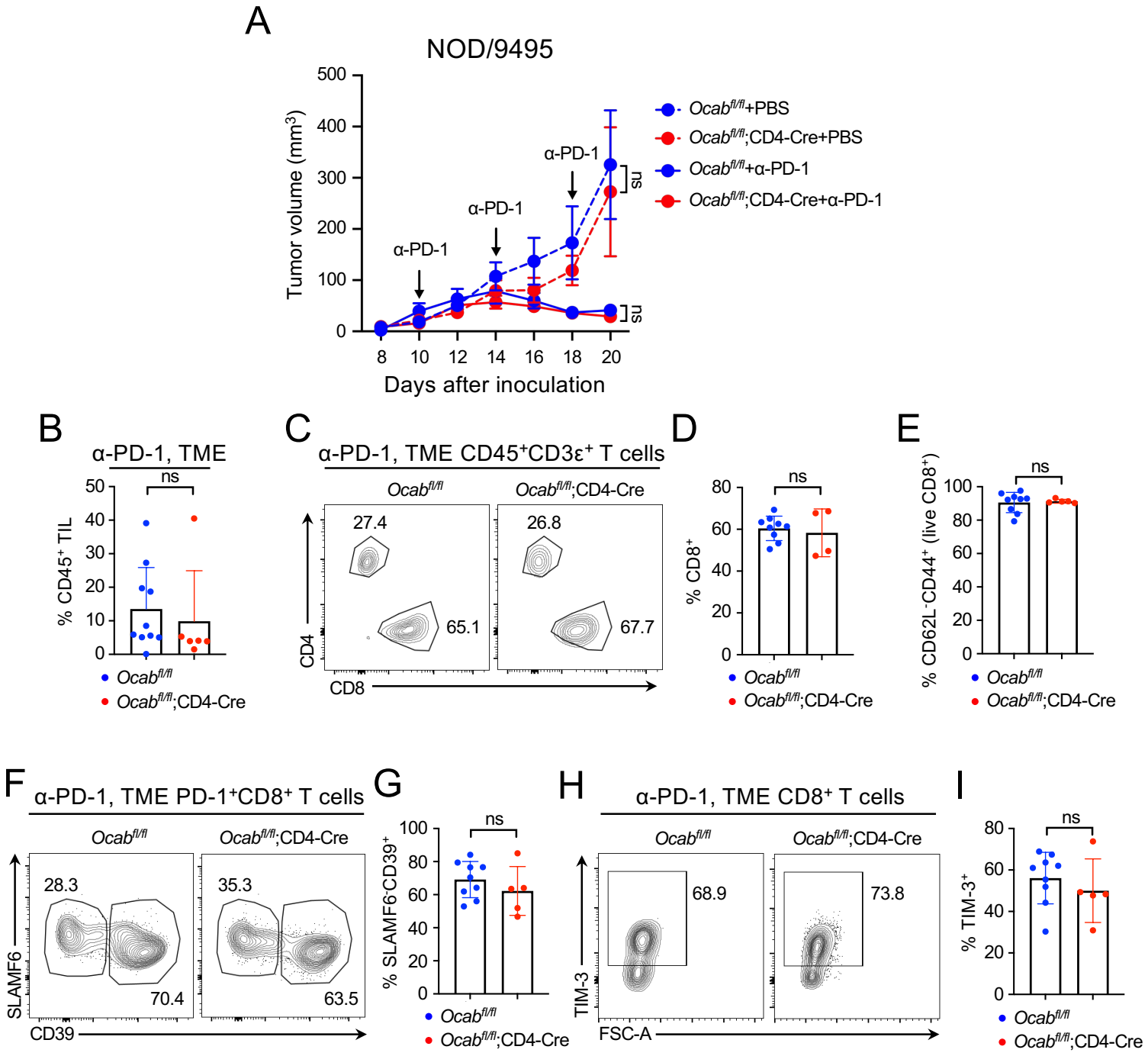

Du et al. Figure 4

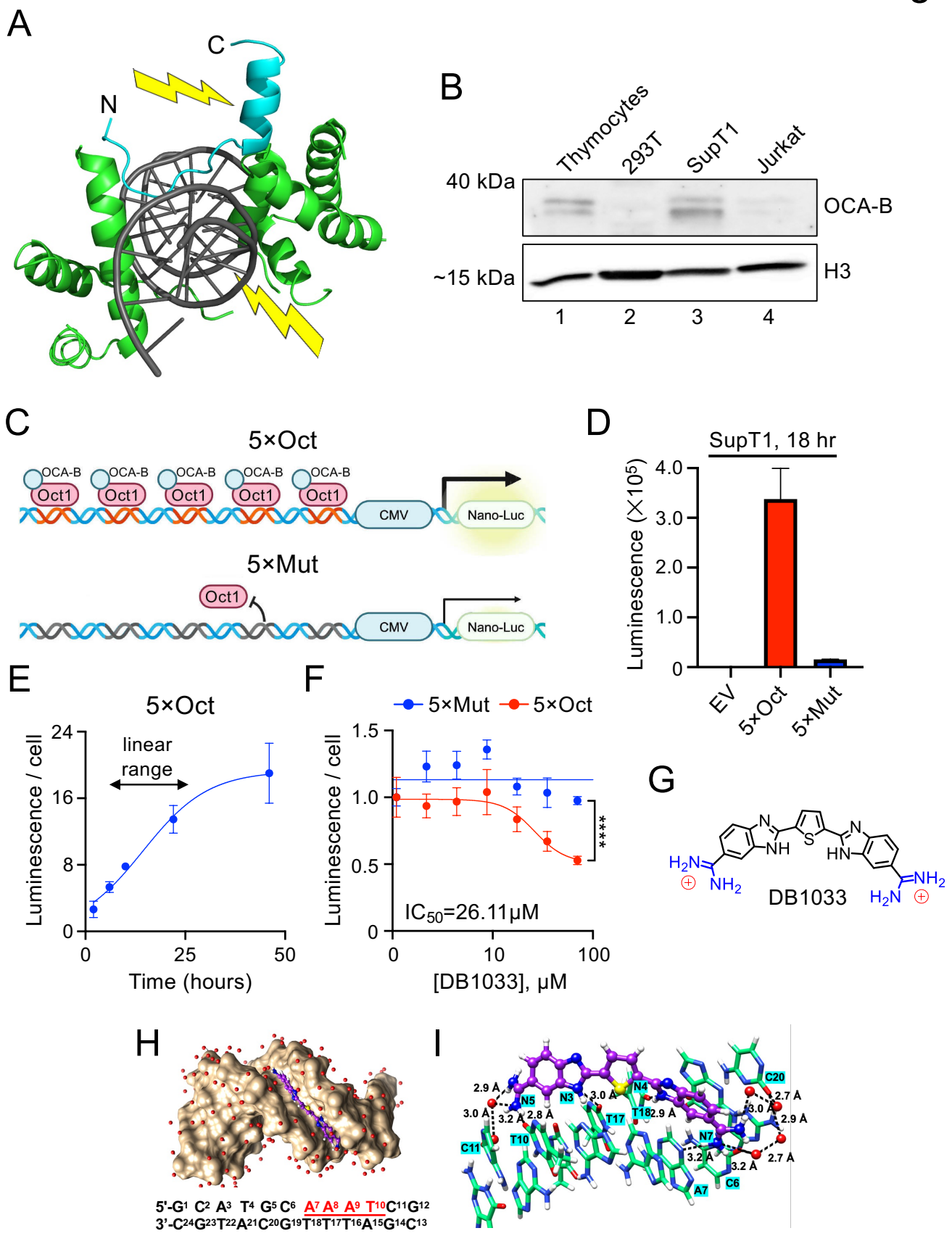

Du et al. Figure 5

A

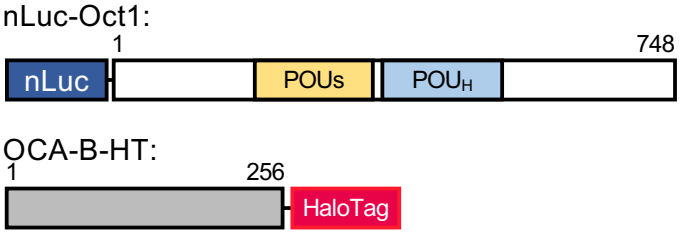

B

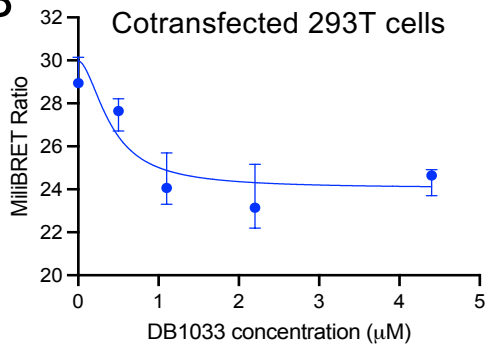

C

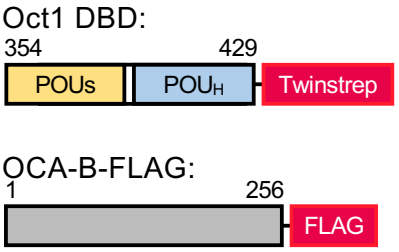

D

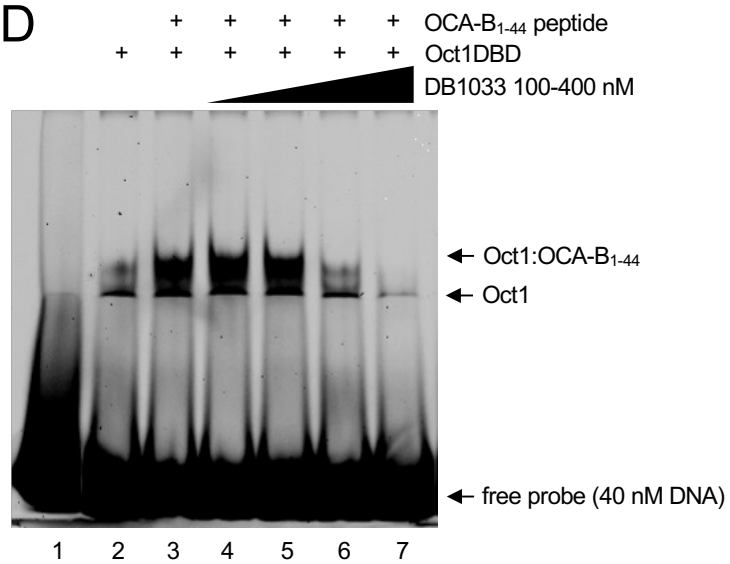

E

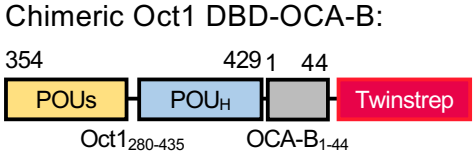

F

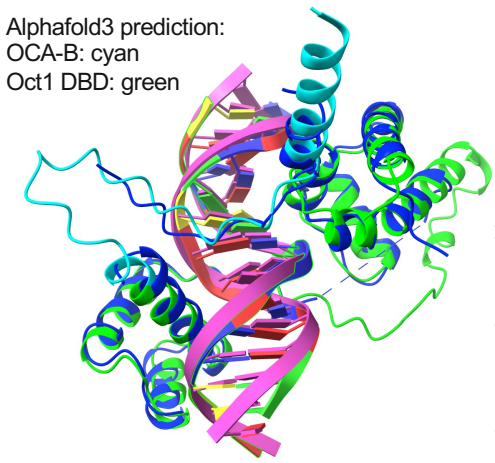

G

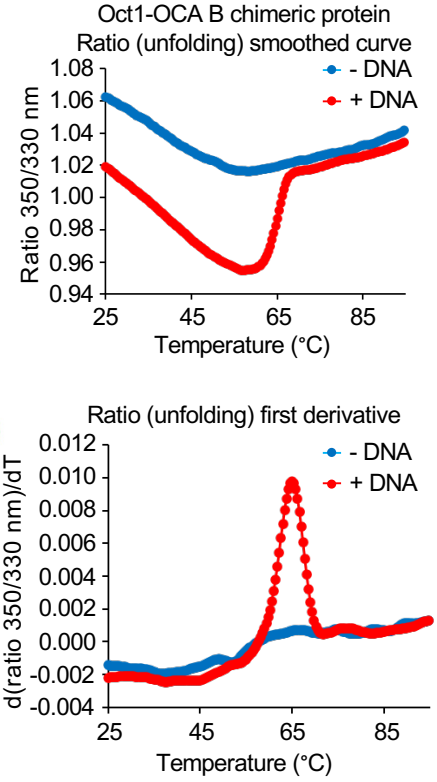

H

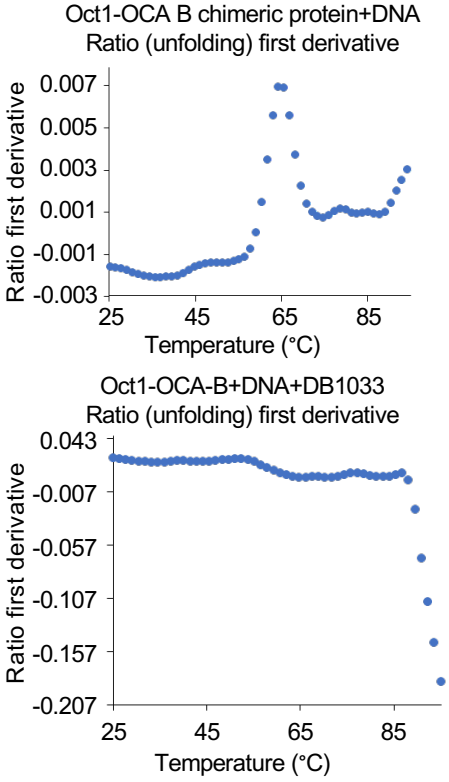
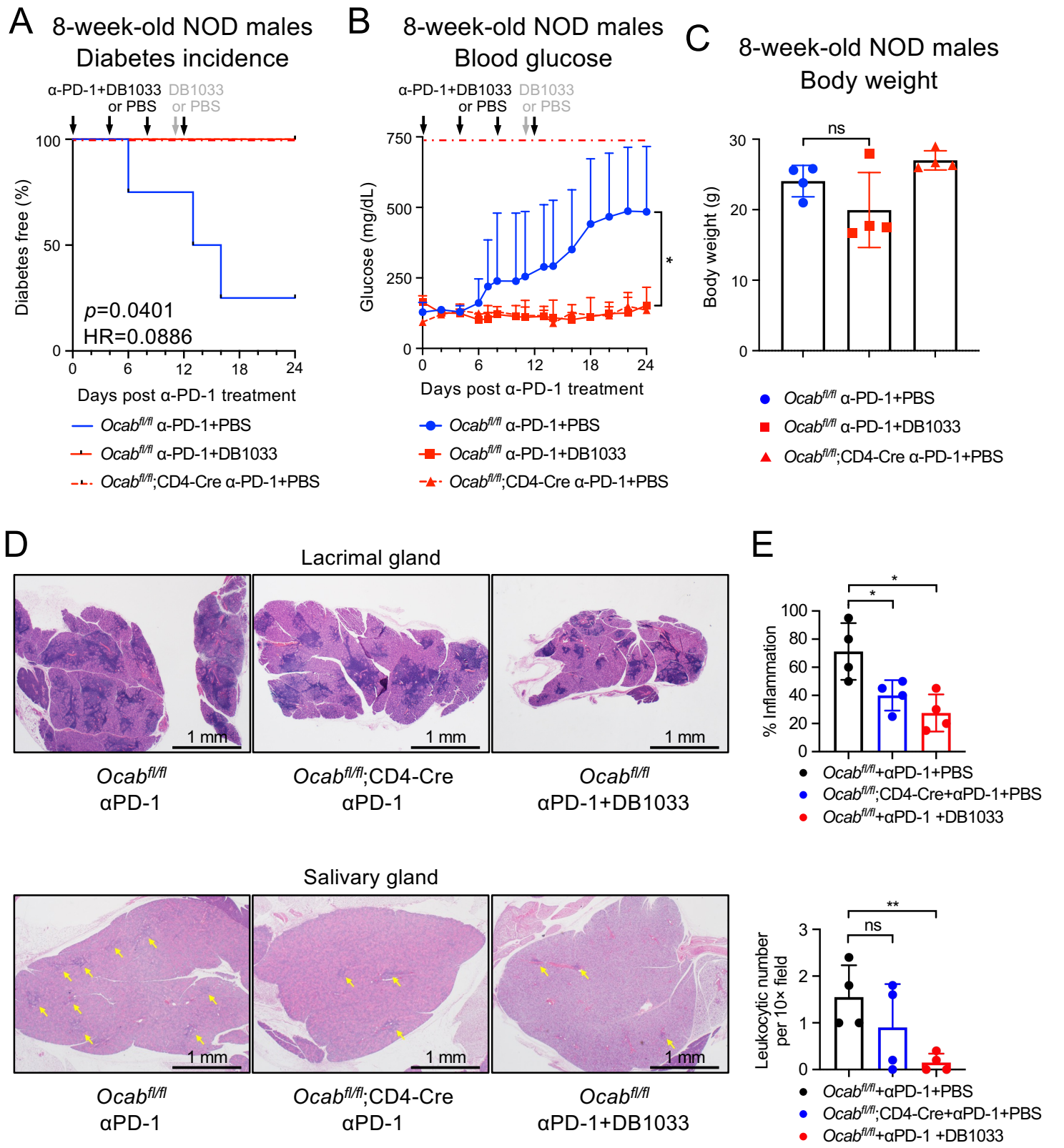
Du et al. Figure 6